# Implications of Bipolar Voltage Mapping and Magnetic Resonance Imaging Resolution in Biventricular Scar Characterization after Myocardial Infarction.

Mariña López-Yunta, MSc[a†], Daniel G. León, MSc[b†], José Manuel Alfonso-Almazán, MSc[b], Manuel Marina-Breysse, MD,[b,c] Jorge G. Quintanilla, MSEng, PhD[b,d,e], Javier Sánchez-González, PhD[f], Carlos Galán-Arriola, DVM[b,e], Victoria Cañadas-Godoy, MD, PhD[d,e], Daniel Enríquez-Vázquez, MD[b,d], Carlos Torres, MD[b,d], Borja Ibáñez, MD, PhD[b,e,g], Julián Pérez-Villacastín, MD, PhD[d,e,h], Nicasio Pérez-Castellano, MD, PhD[d,e], José Jalife, MD[b,e,i], Mariano Vázquez, PhD[a], Jazmín Aguado-Sierra, PhD[a*], David Filgueiras-Rama, MD, PhD[b,d,e*]

†Both authors contributed equally to this work.

* Joint corresponding authors.

[a]Barcelona Supercomputing Center (BSC), Barcelona, Spain.

[b]Centro Nacional de Investigaciones Cardiovasculares Carlos III (CNIC), Myocardial Pathophysiology Area, Madrid, Spain.

[c]Agencia Española de Protección de la Salud en el Deporte (AEPSAD), Madrid. Spain.

[d]Instituto de Investigación Sanitaria del Hospital Clínico San Carlos (IdISSC), Cardiovascular Institute, Madrid, Spain.

[e]CIBER de Enfermedades Cardiovasculares, Madrid, Spain.

[f]Philips Healthcare Iberia, Madrid, Spain.

[g]IIS-University Hospital Fundación Jiménez Díaz, Madrid, Spain.

[h]Fundación Interhospitalaria para la Investigación Cardiovascular (FIC), Madrid, Spain

[i]Center for Arrhythmia Research, Cardiovascular Research Center, Department of Internal Medicine, University of Michigan, Ann Arbor, USA

***Address for correspondence:**

David Filgueiras-Rama. Centro Nacional de Investigaciones Cardiovasculares Carlos III (CNIC), Myocardial Pathophysiology Area. Melchor Fernández Almagro, 3. 28029. Madrid, Spain. Tel: +34 914531200 (Ext. 1510). Fax: +34 914531265. Email: david.filgueiras@cnic.es

Jazmín Aguado-Sierra. Barcelona Supercomputing Center (BSC), Carrer de Jordi Girona, 29-31, 08034, Barcelona, Spain. Email: jazmin.aguado@bsc.es

## ABSTRACT

**Aims:** We aimed to study the differences in biventricular scar characterization using bipolar voltage mapping compared with state-of-the-art *in-vivo* delayed gadolinium-enhanced cardiac magnetic resonance (LGE-CMR) imaging and *ex-vivo* T1 mapping.

**Methods:** Ten pigs with established myocardial infarction (MI) underwent *in-vivo* scar characterization using LGE-CMR imaging and high-density voltage mapping of both ventricles using a 3.5-mm tip catheter. *Ex-vivo* post-contrast T1 mapping provided a high-resolution reference. Voltage maps were registered onto the left and right ventricular (LV and RV) endocardium, and epicardium of CMR-based geometries to compare voltage-derived scars with surface-projected 3D scars.

**Results:** Voltage-derived scar tissue of the LV endocardium and the epicardium resembled surface projections of 3D *in-vivo* and *ex-vivo* CMR-derived scars using 1-mm of surface projection distance. The thinner wall of the RV was especially sensitive to lower resolution *in-vivo* LGE-CMR images, in which differences between normalized low bipolar voltage areas and CMR-derived scar areas did not decrease below a median of 8.84% (interquartile range [IQR] [3.58, 12.70%]). Overall, voltage-derived scars and surface scar projections from *in-vivo* LGE-CMR sequences showed larger normalized scar areas than high-resolution *ex-vivo* images (12.87% [4.59, 27.15%]; 18.51% [11.25, 24.61%], and 9.30% [3.84, 19.59%], respectively), despite having used optimized surface projection distances. Importantly, 43.02% [36.54, 48.72%] of voltage-derived scar areas from the LV endocardium were classified as non-enhanced healthy myocardium using *ex-vivo* CMR imaging.

**Conclusion:** *In-vivo* LGE-CMR sequences and high-density voltage mapping using a conventional linear catheter fail to provide accurate characterization of post-MI scar, limiting the specificity of voltage-based strategies and imaging-guided procedures.

**Keywords:** Magnetic resonance imaging; T1 mapping; myocardial infarction; voltage mapping; myocardial substrate.

## CONDENSED ABSTRACT

High-density voltage mapping of both ventricles correlated with surface scar projections obtained at ~1 mm from the endocardial or epicardial border of 3D cardiac magnetic resonance (CMR)-based reconstructions. Conventional bipolar maps failed to distinguish specific non-enhanced *ex-vivo* T1 mapping-derived healthy areas within low-voltage territories of the left ventricular endocardium.

**What is new?**

- High-density voltage mapping of both ventricles after established myocardial infarction correlates with surface scar projections obtained at ~1 mm from the endocardial or epicardial border of accurate 3D *in-vivo* and *ex-vivo* cardiac magnetic resonance (CMR)-based reconstructions.
- Bipolar maps and state-of-the-art delayed gadolinium-enhanced CMR sequences *in-vivo* fail to distinguish specific areas within low-voltage territories that were identified as non-enhanced healthy myocardium using high-resolution T1 mapping.
- The thinner wall of the right ventricle is especially sensitive to the lower resolution of *in-vivo* CMR images, which is reflected by large differences between normalized voltage-derived scar areas and CMR-derived surface-projected scar areas.
- The specificity of substrate-based strategies and imaging-guided procedures is affected by current standard resolutions of both bipolar voltage mapping using a 3.5-mm tip catheter and *in-vivo* delayed gadolinium-enhanced CMR sequences.

## INTRODUCTION

Scar characterization using different cardiac imaging modalities is a common clinical approach to stratify the risk of ventricular arrhythmia and identify potential target areas for catheter-based ablation after myocardial infarction (MI).[1, 2] Among such imaging techniques, delayed gadolinium-enhanced cardiac magnetic resonance (LGE-CMR) is a well-established method to characterize myocardial structural changes.[3] Voltage mapping is another common approach to identify abnormal electrograms and low voltage areas that may be related to arrhythmogenesis.[2, 4]

Both LGE-CMR imaging and voltage mapping approaches have intrinsic limitations that may affect structural substrate interpretation, and therefore substrate-guided therapeutic interventions. Scar and surviving tissue identification on LGE-CMR sequences are highly affected by current standards on LGE-CMR resolution, and the well-known influence of aliasing and partial volume effects.[5] Moreover, no consensus exists on either a uniform scar evaluation technique or signal intensity thresholding for scar characterization,[1, 6] both of which vary among different series and makes scar characterization particularly sensitive to sampling bias depending on the specific approach. Thus, CMR-based scar characterization remains controversial and has not been incorporated as a standard tool to guide therapeutic interventions.[4, 7]

Voltage-derived scar tissue using a conventional 4-mm tip mapping/ablation catheter and the established cutoff values for defining normal (>1.5 mV) and dense scar myocardium (<0.5 mV) also impose limitations on precise substrate characterization.[4] Among other factors, fiber orientation, catheter contact and fat significantly affect the represented scar.[7, 8] However, voltage-mapping recordings and clinically available LGE-CMR sequences may provide complementary information and valuable clinical input if imaging interpretation is based on appropriate understanding of voltage and signal intensity limitations.

We hypothesize that *in-vivo* LGE-CMR sequences and voltage mapping-derived scar tissue will have limitations, directly related to resolution technique, to identify surviving myocardial regions that can be identified using high-resolution T1 mapping. We compared the differences in scar characterization using 3D voltage maps versus *in-vivo* LGE-CMR and *ex-vivo* post-contrast T1 mapping. We also aimed to optimize the interpretation of *in-vivo* LGE-CMR sequences and voltage-derived maps of both ventricles using *ex-vivo* T1 mapping as a high-resolution reference.

## METHODS

Detailed information of the methodology is provided in the Supplementary Material. Figure 1 summarizes the experimental workflow.

### Pig model of myocardial infarction

The studies were conducted in accordance with institutional guidelines and National and European regulation guidelines for the care and use of laboratory animals. Ten castrated male pigs (large-white strain, ~35 kg) underwent percutaneous catheterization of the left anterior descending (LAD) coronary artery using percutaneous femoral access and fluoroscopic guidance under general anaesthesia. Unfractionated heparin (300 UI/kg) was administered at the onset of the instrumentation. An angioplasty balloon was inflated either proximal (n=5) or distal (n=5) to the first diagonal branch to generate different infarct sizes and variable scar distributions. After 60 minutes of occlusion, the balloon was deflated and a coronary angiogram was recorded to confirm patency of the coronary artery and reperfusion as described elsewhere.[9] After 5 days of recovery, all animals were transferred to specific animal research facilities for 10-12 weeks before CMR studies and invasive cardiac electrophysiology characterization.

### *In-vivo* CMR imaging

One-to-three days before the electrophysiology study all pigs (~55-60 Kg) underwent substrate characterization using a Philips Achieva 3T-Tx whole-body scanner equipped with a 32-element and phased-array cardiac coil (Philips Healthcare, Best, The Netherlands). Ten minutes after intravenous contrast injection (0.2 mM/kg. Dotarem, Guerbet) 3D LGE sequences were acquired using an inversion-recovery spoiled turbo field echo (IR-T1TFE) with isotropic resolution of 1.5x1.5x1.5 $mm^3$.

**Electrophysiology study and voltage-based substrate characterization**

Anaesthesia induction and maintenance were the same as during the MI protocol. The study was performed using percutaneous venous and arterial femoral access to reach the right and left ventricles (RV, LV), respectively. Additional epicardial access was achieved using a subxiphoid percutaneous approach and an 8.5 French epicardial sheath (Agilis EPI 40 cm. St. Jude Medical Inc., St. Paul, MN) positioned on the pericardial space. During sinus rhythm, voltage maps were sequentially generated from the endocardium of the LV, RV and the epicardial surface of both ventricles using a 3.5-mm irrigated-tip mapping catheter (Navistar Thermocool, Biosense Webster, Diamond Bar, CA) and a 3D electroanatomic mapping system (Carto3, Biosense Webster). Acquired bipolar signals were filtered at 30-500 Hz. Surface projection of acquired voltage data was set at 7 mm. Finally, a single intravenous bolus (0.2 mM/kg) of gadolinium-based contrast agent (Dotarem, Guerbet) was administered 10 minutes before euthanasia and heart excision.

***Ex-vivo* CMR imaging**

Right after euthanasia and heart excision, volume-preserved hearts were introduced in a custom-designed, watertight plastic flask containing 2% agarose gel that perfectly adjusted to an 8-channel phased array knee coil. A 3D T1 mapping sequence was acquired using a Look-Locker inversion recovery-turbo field echo sequence (TR/TE/Flip Angle=5.9 ms/2.8 ms/7º) with

acquired isotropic resolution of 0.60x0.60x0.60 $mm^3$. Thirty-six inversion times were acquired with a 147-ms gap between them.

**Voltage maps processing**

Bipolar signals were processed offline using custom-made software in Matlab (MathWorks Inc., Natick, US). Acquired bipolar electrograms were projected towards the electroanatomic mesh nodes using a minimum distance-based criterion. Data interpolation among nodes was performed using the inverse distance-weighted algorithm.[10] Briefly, nodes with unknown data are assigned a weighted linear combination of the neighbouring data-filled nodes.

**Processing of CMR images**

**Scar segmentation from *ex-vivo* R1 images**

R1 images were calculated from the 36-inversion times of T1 images using a customized software (IDL 8.1, Boulder, CO) as published elsewhere.[11] Initial segmentation of the myocardium was performed semiautomatically using custom-made software in Matlab, complemented with fine manual segmentation (~28-30 h per heart). Scar segmentation was performed using a modified strategy based on the full-width-half-maximum method to normalize signal intensity to maximum myocardial signal intensity (Figure S1).[3] All cutoff values from 0.40 to 0.70 of the maximum signal intensity were evaluated to detect the most accurate scar delineation (Figure 2A, B).

**Scar segmentation from *in-vivo* LGE-CMR images**

Similarly, to *ex-vivo* sequences, initial segmentation of the myocardium was performed semiautomatically using custom-made software in Matlab, although a longer time was required for fine manual segmentation (~48 h per heart). Then, scar segmentation was performed using

the same criteria as for *ex-vivo* images without applying any filtering among neighbouring voxels.

**Surface projection of 3D scar regions**

Surface scar projection was performed using distance-to-scar maps that were computed from the segmented ventricular myocardium. The maps were generated with a mathematical tool based on Eikonal equations to calculate scar distances to a given surface (Figure S2).[12] Two types of surface maps were generated for each myocardial territory (LV endocardium, RV endocardium and epicardium) to differentiate between dense and heterogeneous scar areas.

**Voltage maps registration onto CMR geometries**

Each myocardial territory was registered onto the corresponding *in-vivo* and *ex-vivo* CMR geometries. The method consisted of an initial registration of anatomical landmarks manually depicted on each voltage and CMR surface. Then, an iterative closest point algorithm was applied to the resulting surfaces using a rigid transformation method (Figure S3).[13] Finally, bipolar voltage data were integrated on the corresponding endocardial or epicardial CMR geometries using the minimum distance criterion.

**Scar quantification and statistical analysis**

We quantified the voltage-derived scar areas after registration on the corresponding *in-vivo* and *ex-vivo* CMR surfaces, and used a linear interpolation method to define scar and healthy regions based on conventional bipolar thresholds (dense scar: <0.5 mV, and heterogeneous scar: 0.5-1.5 mV as low voltage regions, and healthy myocardium: >1.5 mV).[4] Using the Pearson correlation coefficient we calculated the correlation between low bipolar voltage areas on the original electroanatomic meshes and such scars registered onto the CMR geometries. The Passing-Bablok regression was used to detect any significant difference after registration of voltage-

maps. Comparisons were performed between registered voltage-derived scars and *in-vivo* or *ex-vivo* 3D surface scar projections. Normalized scar tissue was calculated as the percentage of scar on the registered *in-vivo* or *ex-vivo* CMR surface. Differences in scar areas are expressed as absolute values. Low voltage areas on the electroanatomic maps corresponding to valvular annuli were not considered for comparisons with surface scar projections from CMR images. Data are expressed as median and interquartile range [IQR] for quantitative variables. Data normality was assessed with the Shapiro-Wilk test.

## RESULTS

Table 1 lists the resolution differences and geometry areas obtained from each imaging technique. It shows also the number of geometry points generated to construct the voltage maps, the voltage acquisition points for each territory and the acquisition times.

### Dense scar voltage criterion affects substrate characterization

Using a conventional cutoff criterion for dense scar (<0.5 mV) resulted in 5.09% [2.97, 9.86] of the LV endocardium being classified as potentially non-viable myocardium (Figure S4A). A similar percentage of the epicardium was classified as dense scar tissue on the epicardial surface (5.27% [1.34, 6.98%], Figure S4A). However, in the RV endocardium, the percentage of dense scar tissue was substantially lower (0.36% [0.07, 0.74%], Figure S4A). Therefore, the infarct territory mainly affected the LV. Decreasing the dense scar cutoff to ≤0.1mV has been suggested to be more specific to detect unexcitable areas.[7] However, the change considerably decreased dense scar tissue in both the LV endocardium (0.17% [0.00002, 0.65%] and the epicardium (0.025% [0.0002, 0.08%]) (Figure S4B). Scar changes in the RV endocardium were negligible due to small areas of very low voltage (≤0.1 mV) with both criteria (Figure S4B).

### Voltage map registration on CMR surfaces preserves scar distribution

Total scar quantification after voltage maps registration on the *in-vivo* or *ex-vivo* CMR geometries (RV endocardium, LV endocardium and epicardium) strongly correlated with the voltage-derived scar areas obtained on the electroanatomic meshes. $R^2$ values of the Pearson correlation coefficient were 0.94 and 0.94 for *in-vivo* and *ex-vivo* registrations, respectively (Figure S5). Quantification of registered and normalized voltage-derived scar tissue on the *in-vivo* and *ex-vivo* CMR geometries showed a median of 2.3% and 2.0% absolute difference, respectively, without statistical significance from the original voltage-derived scars on the electroanatomic geometry (Figure S6).

**Comparisons of low bipolar voltage areas with surface scar projections from CMR**

Conventional low voltage maps of the LV endocardium started to resemble heterogeneous and dense scar areas from *in-vivo* LGE-CMR at the minimum evaluated (0.5 mm) surface projection distance (Figure 3A). However, scar regions from *ex-vivo* high-resolution CMR images required larger surface projection distances (~1.0 mm) to resemble voltage-derived scar areas (Figure 3B). The data indicate that high-resolution and fine-segmented CMR sequences may potentially distinguish thin surviving endocardial layers, just a few hundred μm thick,[14] which could not be detected using lower resolution techniques. Further analysis supported this assertion since 24.95% [18.92, 36.86%] and 43.02% [36.54, 48.72%] of voltage-derived scar areas in the left ventricular endocardium was classified as non-enhanced healthy myocardium using *in-vivo* LGE-CMR and *ex-vivo* post-contrast T1 mapping, respectively (Figure S7).

Adjusting voltage criteria for dense scar tissue to ≤0.1 mV dramatically decreased voltage derived-dense scar areas (Figure 3C). As a result, neither *in-vivo* nor *ex-vivo* CMR-derived scar areas resembled such small voltage-derived dense scar areas at any of the projection distances (Figure 3C, D).

Epicardial scar areas from *in-vivo* and *ex-vivo* CMR images showed similar patterns, with progressively larger heterogeneous and dense scar areas as the surface projection distance increased (Figure 4A, B). Thus, the epicardium of *in-vivo* and *ex-vivo* CMR images showed small scar areas at 0.5 mm (normalized scar: 2.53% [1.04, 3.11%] and 2.12 [0.48, 4.89%], respectively) of surface projection distance compared with voltage-derived epicardial scar areas (9.93% [7.70%, 20.63%], and 8.70% [7.01, 17.11%] for normalized *in-vivo* and *ex-vivo* voltage map registrations, respectively. Figure 4A, B). The latter highlights the potential effect of fat on epicardial voltage amplitudes,[8] which was minimized in fine epicardial segmentations, especially from *ex-vivo* high-resolution sequences (Figure 4A). Decreasing the dense scar cutoff to ≤0.1 mV almost eliminated the entire epicardial voltage-derived dense scar, (Figure 4C, D) similarly to the effect observed in the LV endocardium (Figure 3C, D).

The much thinner RV wall showed a different scenario, in which endocardial voltage-derived scar areas were consistently smaller than *in-vivo* CMR-derived scar areas at all the surface projection distances (Figure 5A). Scar comparisons using *ex-vivo* high-resolution images showed that RV voltage-maps resembled CMR-derived scar areas at 1 mm of surface projection distance (Figure 5B). Decreasing the dense scar cutoff from <0.5 mV to ≤0.1 mV did not affect comparisons, since changes in normalized voltage-derived dense scar areas were negligible (Figure 5C, D).

**Biventricular scar interpretation using bipolar mapping and CMR imaging**

Normalized total scar areas from *in-vivo* and *ex-vivo* CMR sequences at the 1 mm surface projection distance showed the minimum difference (range 4.0-5.1%) compared with voltage-derived scar areas either from the LV endocardium or the epicardium (Figure 6A, B). Voltage-derived scar areas from the RV were also consistent with the 1 mm surface projection distance using *ex-vivo* CMR images (normalized difference 3.10% [1.65, 6.24%], Figure 6C). However,

the optimal correlation of voltage-derived RV scar areas using lower-resolution images from *in-vivo* LGE-CMR was documented at the minimum (0.5 mm) evaluated surface projection distance (normalized difference 8.84% [3.58, 12.70%]. Figure 6C).

A similar interpretation was also valid for normalized dense scar areas using 0.5 mV as voltage cutoff (Figure S8). The 0.5 mm surface projection distance using *in-vivo* LGE-CMR images showed a slightly smaller difference (4.25% [1.32, 4.63%]) than the 1 mm criterion (9.23% [6.14, 9.82%]) compared with voltage-derived dense scar areas from the LV endocardium.

Overall, biventricular voltage-derived scar areas and surface scar projections from *in-vivo* LGE-CMR sequences showed larger normalized scar areas than *ex-vivo* T1 mapping images (12.87% [4.59, 27.15%], 18.51% [11.25, 24.61%], and 9.30% [3.84, 19.59%], respectively), despite using 1-mm distance for surface projection of CMR-derived scar areas.

**DISCUSSION**

We characterized the voltage-derived MI scar of the entire ventricles using bipolar recordings and a conventional mapping/ablation catheter. The voltage maps correlated with surface scar projections from *in-vivo and ex-vivo* CMR sequences at ~1 mm from the endocardial or epicardial borders. Overall, normalized scar differences among techniques were ~5% using the optimal surface projection distance from CMR sequences. Bipolar recordings provided average information of ~1-mm deep of the mapped territories, which failed to distinguish specific regions within low voltage territories that could be identified as non-enhanced healthy myocardium using high-resolution images. *In-vivo* LGE-CMR sequences showed larger scar areas than *ex-vivo* high-resolution sequences at surface projection distances <1 mm, which demonstrates that partial volume limitations affect lower resolution images, especially in the thinner wall of the RV.

Substrate characterization after MI has been used to guide therapeutic interventions as catheter-based ablation of ventricular tachycardia.[1, 15] Substrate-based procedures are commonly characterized by long radiofrequency delivery times and large ablated areas,[15] which may achieve lower recurrence rates during follow-up compared with a more conservative approach.[15] However, our results indicate that bipolar voltage mapping using a conventional mapping/ablation catheter lacks specificity for detailed scar characterization. Thus, potentially surviving endocardial layers within low voltage areas of the LV endocardium would be classified as scar, even though high-resolution images would identify them as non-enhanced healthy myocardium. Mapping resolution can be increased using multipolar catheters with smaller electrodes size,[16] which reduces the estimated scar extension and identifies regions of viable myocardium within very low voltage areas. However, estimated scar extensions using multipolar catheters and 1-mm electrodes may still provide slightly larger scar areas than *ex-vivo* CMR studies focused on the LV endocardium.[16] Moreover, voltage mapping is not the only criterion to identify abnormal substrates, as electrogram morphology is also affected by catheter electrode size.[7] Thus, multipolar catheters with smaller electrodes may show healthy-looking, sharp and high-voltage electrograms in regions where larger electrode sizes show overt abnormal electrograms.[16]

*In-vivo* LGE-CMR has been used also to identify the abnormal substrate and conduction channels based on signal intensity criteria.[1, 17] However, our results demonstrate that even state-of-the-art *in-vivo* 3D sequences are limited in the ability to identify areas of normal tissue within heterogeneous or dense scar areas. The latter is reflected by the larger normalized scar regions estimated from *in-vivo* sequences at surface projection distances <1 mm compared with *ex-vivo* CMR-derived scar areas. Such differences are related to larger partial volume effects in lower resolution images,[5] which become even more relevant in thinner structures such as the RV wall (Figure 5). Importantly, scar areas quantification using two different techniques may

resemble each other at surface projection distances closer to *in-vivo* CMR resolutions and electrode size resolutions. However, this does not mean that the underlying complex substrate can be properly identified as demonstrated with higher resolution *ex-vivo* sequences. Moreover, substrate characterization using LGE-CMR images is also affected by signal intensity thresholding, which varies among series and there is a lack of uniform consensus on the methodology to classify scar tissue.[1, 6, 17] Therefore, tissue classification as healthy, heterogeneous or dense scar is particularly sensitive to sampling bias, which would substantially change imaging interpretation of viable tissue and potential conduction channels within scar areas. Altogether the foregoing explains why CMR-based scar tissue characterization remains controversial and has not been incorporated as a standard tool to guide ablation in clinical practice.[18] We have minimized such imaging limitations using highly precise and time-consuming (~28-48 h) whole heart myocardial segmentations along with comprehensive characterization of signal intensity thresholdings from *in-vivo* and *ex-vivo* sequences before selecting specific criteria (Figure 2). The latter enabled us to understand not only frequently obtained results using different imaging approaches, but more importantly specific technical limitations that may affect clinical interpretation.

Despite limitations, clinical substrate-based ablation procedures may benefit from incorporating CMR-derived 3D reconstructions of patient-specific infarct-related substrates in electroanatomical mapping systems. Importantly, surface scar projections should be obtained after accurate myocardial segmentation using the 1-mm distance criterion. The latter will aid cardiac electrophysiologists to localize the region of interest (e.g. endocardium or epicardium) and plan the procedure accordingly. Imaging data in combination with bipolar voltage mapping using multipolar catheters with small electrodes size (0.4-1 mm) will substantially improve substrate characterization within the infarct territory.[16] However, other details like identification

of potential ventricular tachycardia channels based on relatively large and manual variations in signal intensity thresholds for scar characterization,[1] will be sensitive to lack of specificity.

Substrate characterization and 3D patient/animal-specific reconstructions have been also used to generate computational models aiming at predicting arrhythmia risk or target areas during ventricular tachycardia ablation.[19] In such models scar segmentation and tissue characterization are crucial steps, since electrophysiological properties assigned to healthy, dense scar or heterogeneous scar regions will be substantially different.[19] In fact, the morphology and size of the heterogeneous scar areas have been described as the main determinants of 3D reentrant locations and the number of potential reentrant sources.[19, 20] Therefore, current LGE-CMR sequences may have important limitations to accurately reconstruct patient-specific substrates, specially using 2D sequences and low resolution acquisitions,[19] which are more sensitive to partial volume effects.[5] The latter would theoretically affect the computational scenarios; therefore any related potential therapeutic strategy. Such weaknesses notwithstanding, CMR technology is rapidly improving and soon will probably allow for briefer acquisition times and higher-resolution sequences, which will also improve the performance and clinical value of computational models.

**Limitations**

Histopathology analyses were not performed to confirm the presence of viable myocardial tracts within voltage-derived dense scar regions. However, it is not surprising to observe that small layers of viable myocardium would not be detected with low resolution techniques (i.e. bipolar mapping using a 3.5-mm tip catheter or *in-vivo* LGE-CMR) compared with high-resolution *ex-vivo* CMR imaging or multipolar catheters with small electrodes size.[5, 16] Relatively large areas of epicardial fat are common in patients with structural heart disease,[8] while in the pig model such areas were mainly limited to the interventricular course of the LAD coronary artery

(Figure 6B). Lower epicardial fat content may have favoured epicardial substrate characterization using i*n-vivo* LGE-CMR compared with other scenarios in the presence of larger fatty areas. CMR sequences using fat suppression or computed tomography studies can provide additional value to increase CMR-based scar characterization in the epicardium.[8]

Although *ex-vivo* CMR studies provided detailed characterization of the underlying ventricular scar tissue after MI, the sequences may still have limitations in thinner myocardial walls such as the atria. Therefore, future studies should address the optimal resolutions during acquisition to achieve consistent and comparable results among series.

## CONCLUSIONS

Current state-of-the-art *in-vivo* LGE-CMR sequences and high-density catheter-based voltage mapping using standard linear mapping/ablation catheters show limitations to provide detailed characterization of post-MI scar tissue compared with high-resolution *ex-vivo* post-contrast T1 mapping. The latter has implications on substrate-based strategies and imaging-guided procedures, which may reflect the lack of specificity.

## ACKNOWLEDGEMENTS

We thank the technical support of all staff members at the animal facilities in CNIC. The CNIC (Madrid, Spain) is supported by the Ministry of Economy, Industry and Competitiveness (MEIC) and the Pro CNIC Foundation. The CNIC and the BSC (Barcelona, Spain) are Severo Ochoa Centers of Excellence (SEV-2015-0505 and SEV-2011-0067, respectively). This study was supported by grants from Instituto de Salud Carlos III, Fondo Europeo de Desarrollo Regional (RD12/0042/0036, CB16/11/00458), Spanish Ministry of Economy and Competitiveness (MINECO) (SAF2016-80324-R, PI16/02110, and DTS17/00136), and by the European Commission (ERA-CVD Joint Call (JTC2016/APCIN-ISCIII-2016), grant#AC16/00021). The study was also partially supported by the Fundación Interhospitalaria

para la Investigación Cardiovascular (FIC, Madrid, Spain) and the Spanish Society of Cardiology (DFR). Dr. Jalife is supported by R01 Grant HL122352 from the National Heart Lung and Blood Institute, USA National Institutes of Health. JAS is funded by the CompBioMed project, H2020-EU.1.4.1.3 European Union's Horizon 2020 research and innovation program, grant#675451. DGL has received financial support through the "la Caixa" Fellowship Grant for Doctoral Studies, "la Caixa" Banking Foundation, Barcelona, Spain.

## REFERENCES

[1]Andreu D, Penela D, Acosta J, Fernandez-Armenta J, Perea RJ, Soto-Iglesias D, et al. Cardiac magnetic resonance-aided scar dechanneling: Influence on acute and long-term outcomes. *Heart Rhythm* 2017; **14**: 1121-8.

[2]Nuhrich JM, Kaiser L, Akbulak RO, Schaffer BN, Eickholt C, Schwarzl M, et al. Substrate characterization and catheter ablation in patients with scar-related ventricular tachycardia using ultra high-density 3-D mapping. *J Cardiovasc Electrophysiol* 2017; **28**: 1058-67.

[3]Amado LC, Gerber BL, Gupta SN, Rettmann DW, Szarf G, Schock R, et al. Accurate and objective infarct sizing by contrast-enhanced magnetic resonance imaging in a canine myocardial infarction model. *J Am Coll Cardiol* 2004; **44**: 2383-9.

[4]Santangeli P, Marchlinski FE. Substrate mapping for unstable ventricular tachycardia. *Heart Rhythm* 2016; **13**: 569-83.

[5]Schuleri KH, Centola M, George RT, Amado LC, Evers KS, Kitagawa K, et al. Characterization of peri-infarct zone heterogeneity by contrast-enhanced multidetector computed tomography: a comparison with magnetic resonance imaging. *J Am Coll Cardiol* 2009; **53**: 1699-707.

[6]Flett AS, Hasleton J, Cook C, Hausenloy D, Quarta G, Ariti C, et al. Evaluation of techniques for the quantification of myocardial scar of differing etiology using cardiac magnetic resonance. *JACC Cardiovasc Imaging* 2011; **4**: 150-6.

[7]Josephson ME, Anter E. Substrate Mapping for Ventricular Tachycardia Assumptions and Misconceptions. *JACC: Clinical Electrophysiology* 2015; **1**: 341-52.

[8]Piers SR, van Huls van Taxis CF, Tao Q, van der Geest RJ, Askar SF, Siebelink HM, et al. Epicardial substrate mapping for ventricular tachycardia ablation in patients with non-ischaemic cardiomyopathy: a new algorithm to differentiate between scar and viable myocardium developed by simultaneous integration of computed tomography and contrast-enhanced magnetic resonance imaging. *Eur Heart J* 2013; **34**: 586-96.

[9]Fernandez-Jimenez R, Sanchez-Gonzalez J, Aguero J, Garcia-Prieto J, Lopez-Martin GJ, Garcia-Ruiz JM, et al. Myocardial edema after ischemia/reperfusion is not stable and follows a bimodal pattern: imaging and histological tissue characterization. *J Am Coll Cardiol* 2015; **65**: 315-23.

[10] Lloyd CD. Assessing the effect of integrating elevation data into the estimation of monthly precipitation in Great Britain. *J Hydrol* 2005; **308**: 128-50.

[11] Messroghli DR, Radjenovic A, Kozerke S, Higgins DM, Sivananthan MU, Ridgway JP. Modified Look-Locker inversion recovery (MOLLI) for high-resolution T1 mapping of the heart. *Magn Reson Med* 2004; **52**: 141-6.

[12] Sethian JA. A fast marching level set method for monotonically advancing fronts. *Proc Natl Acad Sci U S A* 1996; **93**: 1591-5.

[13] Besl PJ, McKay ND. A method for registration of 3-D shapes. *IEEE Transactions on Pattern Analysis and Machine Intelligence* 1992; **14**: 239-56.

[14] Tschabrunn CM, Roujol S, Nezafat R, Faulkner-Jones B, Buxton AE, Josephson ME, et al. A swine model of infarct-related reentrant ventricular tachycardia: Electroanatomic, magnetic resonance, and histopathological characterization. *Heart Rhythm* 2016; **13**: 262-73.

[15] Di Biase L, Santangeli P, Burkhardt DJ, Bai R, Mohanty P, Carbucicchio C, et al. Endo-epicardial homogenization of the scar versus limited substrate ablation for the treatment of electrical storms in patients with ischemic cardiomyopathy. *J Am Coll Cardiol* 2012; **60**: 132-41.

[16] Tschabrunn CM, Roujol S, Dorman NC, Nezafat R, Josephson ME, Anter E. High-Resolution Mapping of Ventricular Scar: Comparison Between Single and Multielectrode Catheters. *Circ Arrhythm Electrophysiol* 2016; **9**.

[17] Perez-David E, Arenal A, Rubio-Guivernau JL, del Castillo R, Atea L, Arbelo E, et al. Noninvasive identification of ventricular tachycardia-related conducting channels using contrast-enhanced magnetic resonance imaging in patients with chronic myocardial infarction: comparison of signal intensity scar mapping and endocardial voltage mapping. *J Am Coll Cardiol* 2011; **57**: 184-94.

[18] Al-Khatib SM, Stevenson WG, Ackerman MJ, Bryant WJ, Callans DJ, Curtis AB, et al. 2017 AHA/ACC/HRS Guideline for Management of Patients With Ventricular Arrhythmias and the Prevention of Sudden Cardiac Death: Executive Summary: A Report of the American College of Cardiology/American Heart Association Task Force on Clinical Practice Guidelines and the Heart Rhythm Society. *Circulation* 2017.

[19] Arevalo HJ, Vadakkumpadan F, Guallar E, Jebb A, Malamas P, Wu KC, et al. Arrhythmia risk stratification of patients after myocardial infarction using personalized heart models. *Nature communications* 2016; **7**: 11437.

[20] Ringenberg J, Deo M, Filgueiras-Rama D, Pizarro G, Ibanez B, Peinado R, et al. Effects of fibrosis morphology on reentrant ventricular tachycardia inducibility and simulation fidelity in patient-derived models. *Clin Med Insights Cardiol* 2014; **8**: 1-13.

**Table 1. Characteristics of each imaging technique.**

| | Voltage mapping | *In-vivo* CMR | *Ex-vivo* CMR |
|---|---|---|---|
| **Technique resolution (mm)** | Catheter tip-ring: 3.5-1 | | |
| Acquisition | | 1.50x1.50x1.50 | 0.60x0.60x0.60 |
| Reconstruction | | 0.57x0.57x0.75 | 0.45x0.45x0.45 |
| **Geometry areas ($cm^2$)**: | | | |
| LV endocardium | **169.50** (163.00, 182.80) | **157.00** (143.00, 166.20) | **149.50** (130.20, 176.00) |
| RV endocardium | **141.50** (137.80, 153.00) | **139.00** (124.20, 147.80) | **167.50** (144.20, 187.50) |
| Epicardium | **203.00** (186.00, 213.20) | **253.50** (232.00, 274.50) | **258.00** (137.0, 292.50) |
| **Geometry points** | | | |
| LV endocardium | **3043** (2922, 3840) | - | - |
| RV endocardium | **3220** (3018, 3574) | - | - |
| Epicardium | **14951** (14014, 16000) | - | - |
| **Voltage acquisition points** | | | |
| LV endocardium | **1123** (1064, 1172) | - | - |
| RV endocardium | **370** (324, 407) | - | - |
| Epicardium | **1112** (1059, 1218) | - | - |
| **Acquisition time (min)** | **167** (149, 191) | **10** | **50** |

Data are expressed as median and interquartile range. CMR: cardiac magnetic resonance. LV: left ventricle. RV: right ventricle.

**FIGURE LEGENDS**

**Figure 1. Experimental workflow. A,** *in-vivo* and *ex*-vivo imaging modalities for biventricular scar characterization. **B,** 3D scar reconstructions obtained from each imaging modality. **C, D,** surface scar projections on the *in-vivo* **(C)** and *ex-vivo* **(D)** CMR-based geometries, and voltage-derived maps registered onto the endocardial and epicardial CMR geometries for comparisons. CMR: cardiac magnetic resonance. ENDO: endocardium. EPI: epicardium. LV: left ventricle. RV: right ventricle.

**Figure 2. Myocardial and scar segmentation process. A,** sample case of myocardial and scar segmentations from *in-vivo* LGE-CMR images (left column) and *ex-vivo* R1 images (right column). **B,** median (colour-coded lines) and interquartile range (colour-coded shadows) of normalized percentage scar areas in each CMR slide at different signal intensity thresholds for *in-vivo* and *ex-vivo* images. Remote scar tissue (outside the infarct region), especially in *ex-vivo* images, rapidly decreased from 0.40 to 0.45 cut-points of maximum signal intensity, which indicated the presence of false positive scar tissue and aided to establish the appropriate cutoff value for scar tissue.

**Figure 3. Left ventricular scar comparisons between registered voltage maps and CMR images. A, B,** left panel, representative case of surface scar projections from *in-vivo* (A) and *ex-vivo* (B) CMR images, and registered voltage maps (mid panel) using a very low voltage cutoff <0.5 mV onto the left ventricular geometries. On the right, surface scar projections of dense and heterogeneous scars at different projection distances from the endocardial border of *in-vivo* (A) and *ex-vivo* (B) CMR images. The median (red and green lines) and interquartile range (red and green shadows) of registered very low and low voltage-derived scars (<0.5 mV and <1.5 mV, respectively) are also represented. **C, D,** left panel, same representative registered voltage maps as in **A** *(in-vivo geometry)***, B** (ex-vivo geometry), using a very low voltage cutoff ≤0.1 mV. On

the right, same data as in **A, B** using the ≤0.1mV cutoff criterion for very low voltage derived-scars. Right panels show data from the entire group of animals (N=10). Ao: aorta. MA: mitral annulus.

**Figure 4. Epicardial scar comparisons between registered voltage maps and CMR images. A, B,** left panel, representative case of surface scar projections from *in-vivo* (A) and *ex-vivo* (B) CMR images, and registered voltage maps (mid panel) using a very low voltage cutoff <0.5 mV onto the epicardial geometries. On the right, surface scar projections of dense and heterogeneous scars at different projection distances from the epicardial border of *in-vivo* (A) and *ex-vivo* (B) CMR images. The median (red and green lines) and interquartile range (red and green shadows) of registered very low and low voltage-derived scars (<0.5 mV and <1.5 mV, respectively) are also represented. **C, D,** left panel, same representative registered voltage maps as in **A** *(in-vivo geometry)***, B** (ex-vivo geometry), using a very low voltage cutoff ≤0.1 mV. On the right, same data as in **A, B** using the ≤0.1mV cutoff criterion for very low voltage derived-scars. Right panels show data from the entire group of animals (N=10).

**Figure 5. Right ventricular scar comparisons between registered voltage maps and CMR images. A, B,** left panel, representative case of surface scar projections from *in-vivo* (A) and *ex-vivo* (B) CMR images, and registered voltage maps (mid panel) using a very low voltage cutoff <0.5 mV onto the right ventricular geometries. On the right, surface scar projections of dense and heterogeneous scars at different projection distances from the endocardial border of *in-vivo* (A) and *ex-vivo* (B) CMR images. The median (red and green lines) and interquartile range (red and green shadows) of registered very low and low voltage-derived scars (<0.5 mV and <1.5 mV, respectively) are also represented. **C, D,** left panel, same representative registered voltage maps as in **A** *(in-vivo geometry)***, B** (ex-vivo geometry), using a very low voltage cutoff ≤0.1 mV. On the right, same data as in **A, B** using the ≤0.1mV cutoff criterion for very low voltage

derived-scars. Right panels show data from the entire group of animals (N=10). RVOT: right ventricular outflow tract. TA: tricuspid annulus.

**Figure 6. Scar differences among registered voltage maps and CMR images at different surface projection distances. A, B, C,** left panels, overlapping scar regions (in green) between registered voltage maps onto the *in-vivo* and *ex-vivo* CMR geometries (A, LV; B, epicardium, C, RV) and CMR-derived scars. No overlapping scar regions, either voltage-derived or CMR-derived, are shown in blue. Right columns show normalized total scar differences (|voltage-derived scar – surface projected CMR scar| / LV, RV or epicardial surface) using sequential surface projection distances from *in-vivo* and *ex-vivo* CMR images. CMR: cardiac magnetic resonance. LV: Left ventricle. RV: Right ventricle.

**Figure 1**

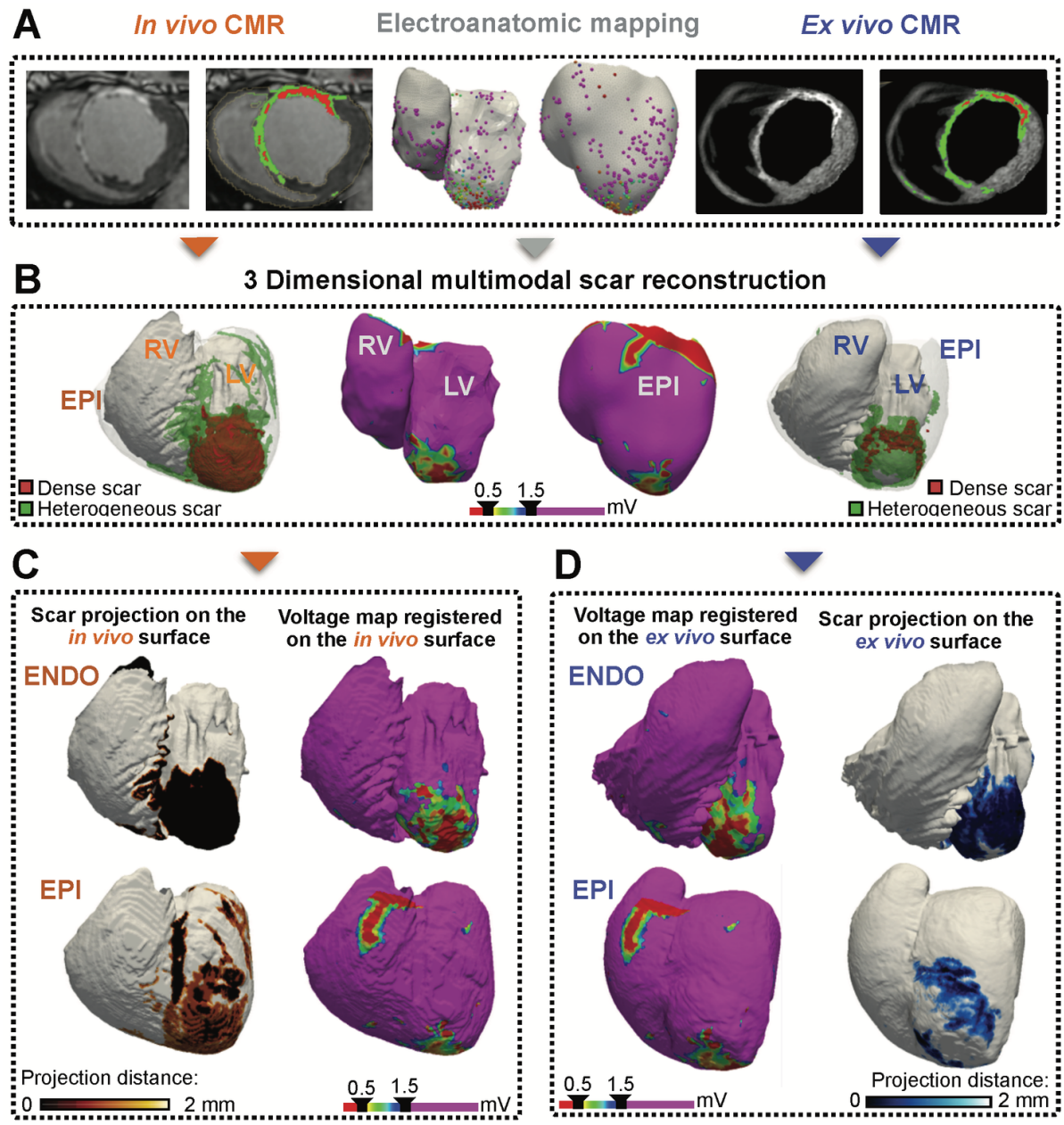
A
In vivo CMR
Electroanatomic mapping
Ex vivo CMR
B
3 Dimensional multimodal scar reconstruction
RV
LV
EPI
Dense scar
Heterogeneous scar
0.5 1.5
mV
C
Scar projection on the in vivo surface
Voltage map registered on the in vivo surface
ENDO
EPI
Projection distance:
0
2 mm
D
Voltage map registered on the ex vivo surface
Scar projection on the ex vivo surface

**Figure 2**

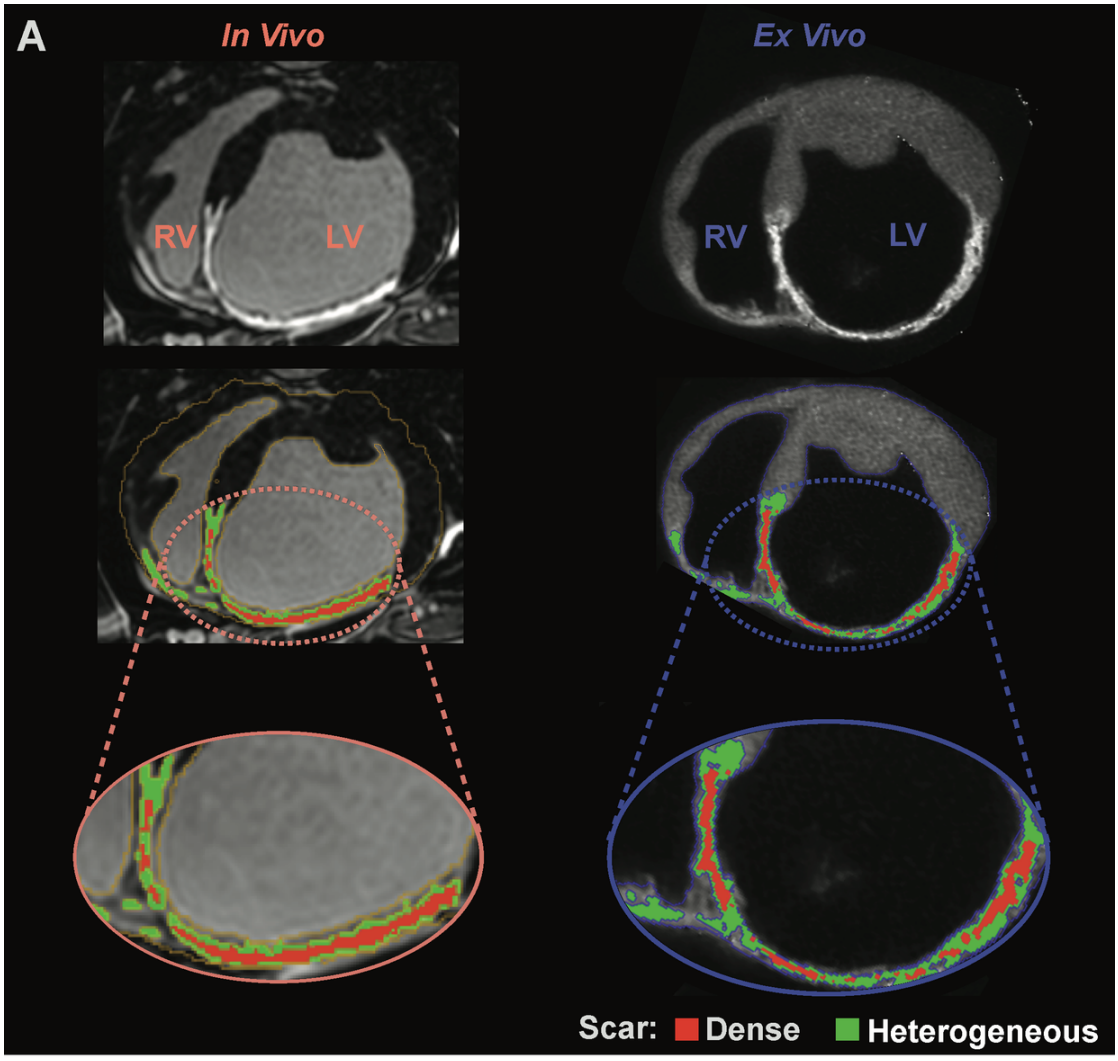
A
In Vivo
Ex Vivo
RV
LV
RV
LV
Scar: Dense Heterogeneous

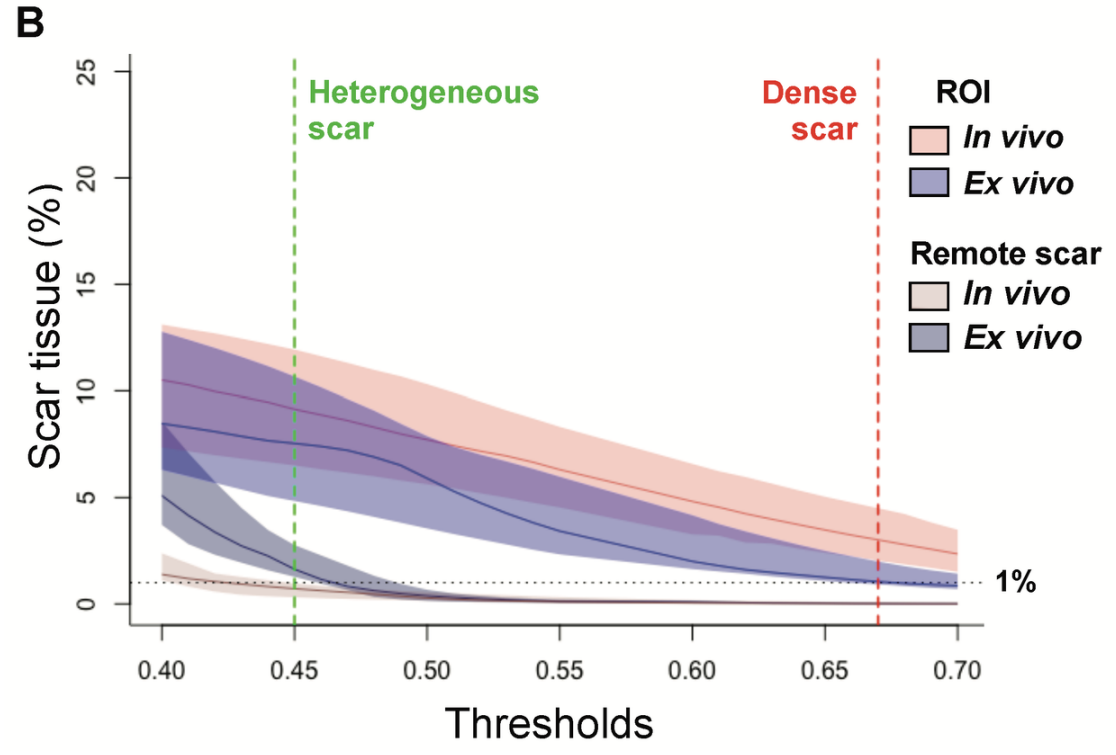
B
Heterogeneous scar
Dense scar
ROI
In vivo
Ex vivo
Remote scar
In vivo
Ex vivo
1%
Scar tissue (%)
0
5
10
15
20
25
0.40
0.45
0.50
0.55
0.60
0.65
0.70
Thresholds

**Figure 3**

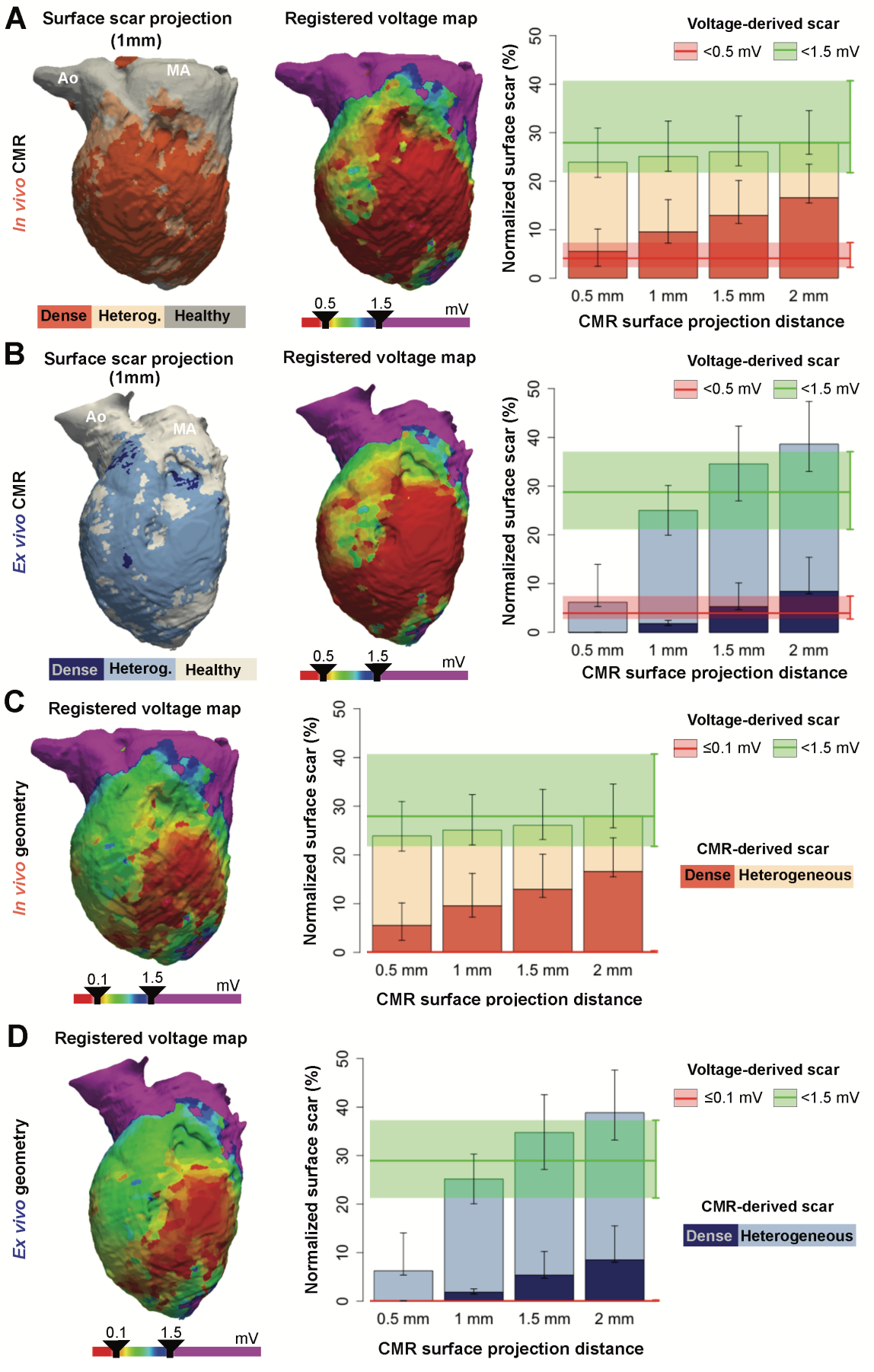
A
Surface scar projection (1mm)
Registered voltage map
In vivo CMR
Ao
MA
Dense
Heterog.
Healthy
0.5
1.5
mV
Voltage-derived scar
<0.5 mV
<1.5 mV
Normalized surface scar (%)
0.5 mm
1 mm
1.5 mm
2 mm
CMR surface projection distance
B
Surface scar projection (1mm)
Registered voltage map
Ex vivo CMR
Ao
MA
Dense
Heterog.
Healthy
0.5
1.5
mV
Voltage-derived scar
<0.5 mV
<1.5 mV
Normalized surface scar (%)
0.5 mm
1 mm
1.5 mm
2 mm
CMR surface projection distance
C
Registered voltage map
In vivo geometry
0.1
1.5
mV
Voltage-derived scar
≤0.1 mV
<1.5 mV
CMR-derived scar
Dense
Heterogeneous
Normalized surface scar (%)
0.5 mm
1 mm
1.5 mm
2 mm
CMR surface projection distance
D
Registered voltage map
Ex vivo geometry
0.1
1.5
mV
Voltage-derived scar
≤0.1 mV
<1.5 mV
CMR-derived scar
Dense
Heterogeneous
Normalized surface scar (%)
0.5 mm
1 mm
1.5 mm
2 mm
CMR surface projection distance

**Figure 4**

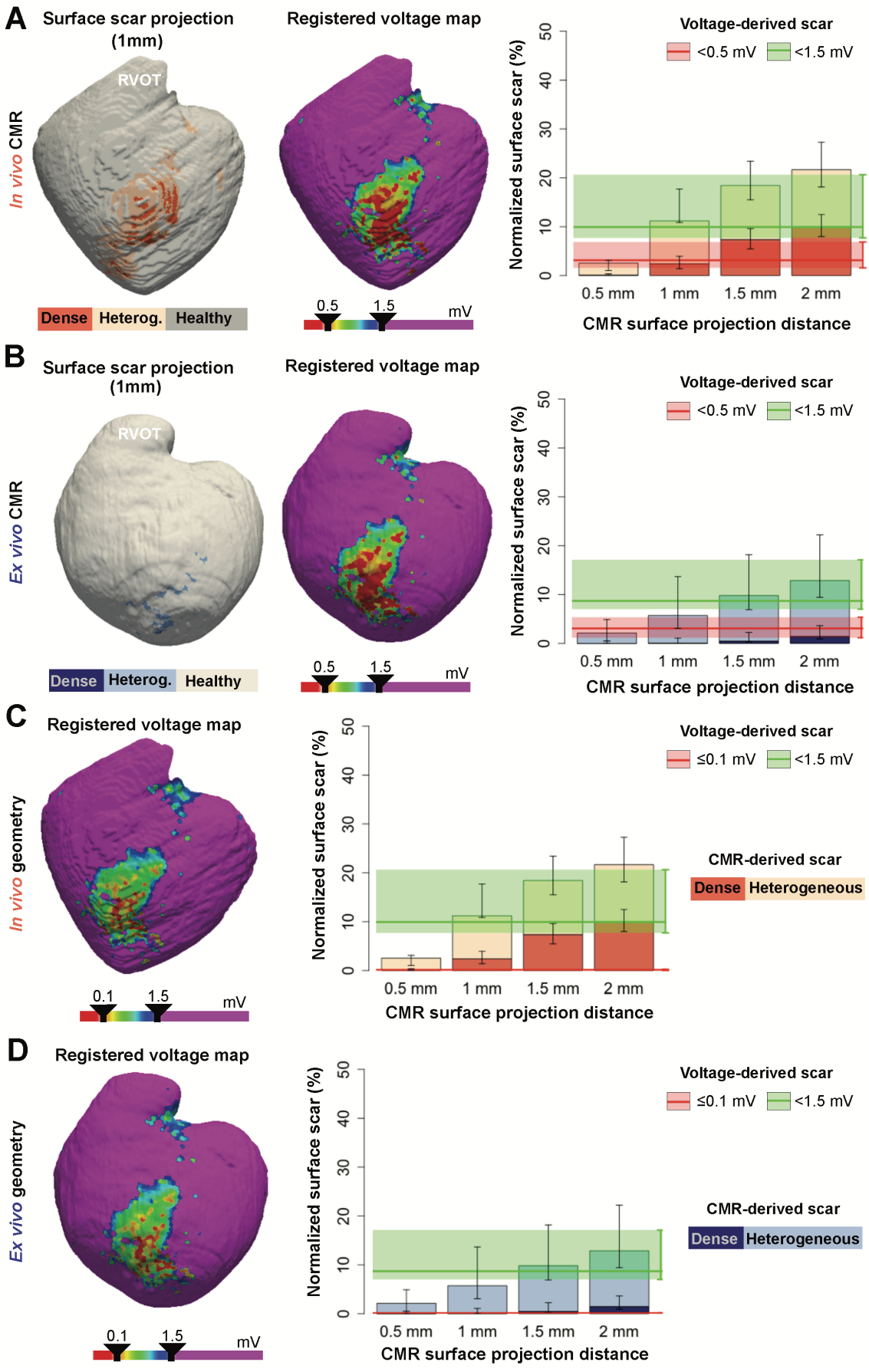
A
Surface scar projection (1mm)
Registered voltage map
In vivo CMR
RVOT
Dense
Heterog.
Healthy
0.5
1.5
mV
Voltage-derived scar
<0.5 mV
<1.5 mV
Normalized surface scar (%)
0.5 mm
1 mm
1.5 mm
2 mm
CMR surface projection distance
B
Surface scar projection (1mm)
Registered voltage map
Ex vivo CMR
RVOT
Dense
Heterog.
Healthy
0.5
1.5
mV
Voltage-derived scar
<0.5 mV
<1.5 mV
Normalized surface scar (%)
0.5 mm
1 mm
1.5 mm
2 mm
CMR surface projection distance
C
Registered voltage map
In vivo geometry
0.1
1.5
mV
Voltage-derived scar
≤0.1 mV
<1.5 mV
CMR-derived scar
Dense
Heterogeneous
Normalized surface scar (%)
0.5 mm
1 mm
1.5 mm
2 mm
CMR surface projection distance
D
Registered voltage map
Ex vivo geometry
0.1
1.5
mV
Voltage-derived scar
≤0.1 mV
<1.5 mV
CMR-derived scar
Dense
Heterogeneous
Normalized surface scar (%)
0.5 mm
1 mm
1.5 mm
2 mm
CMR surface projection distance

**Figure 5**

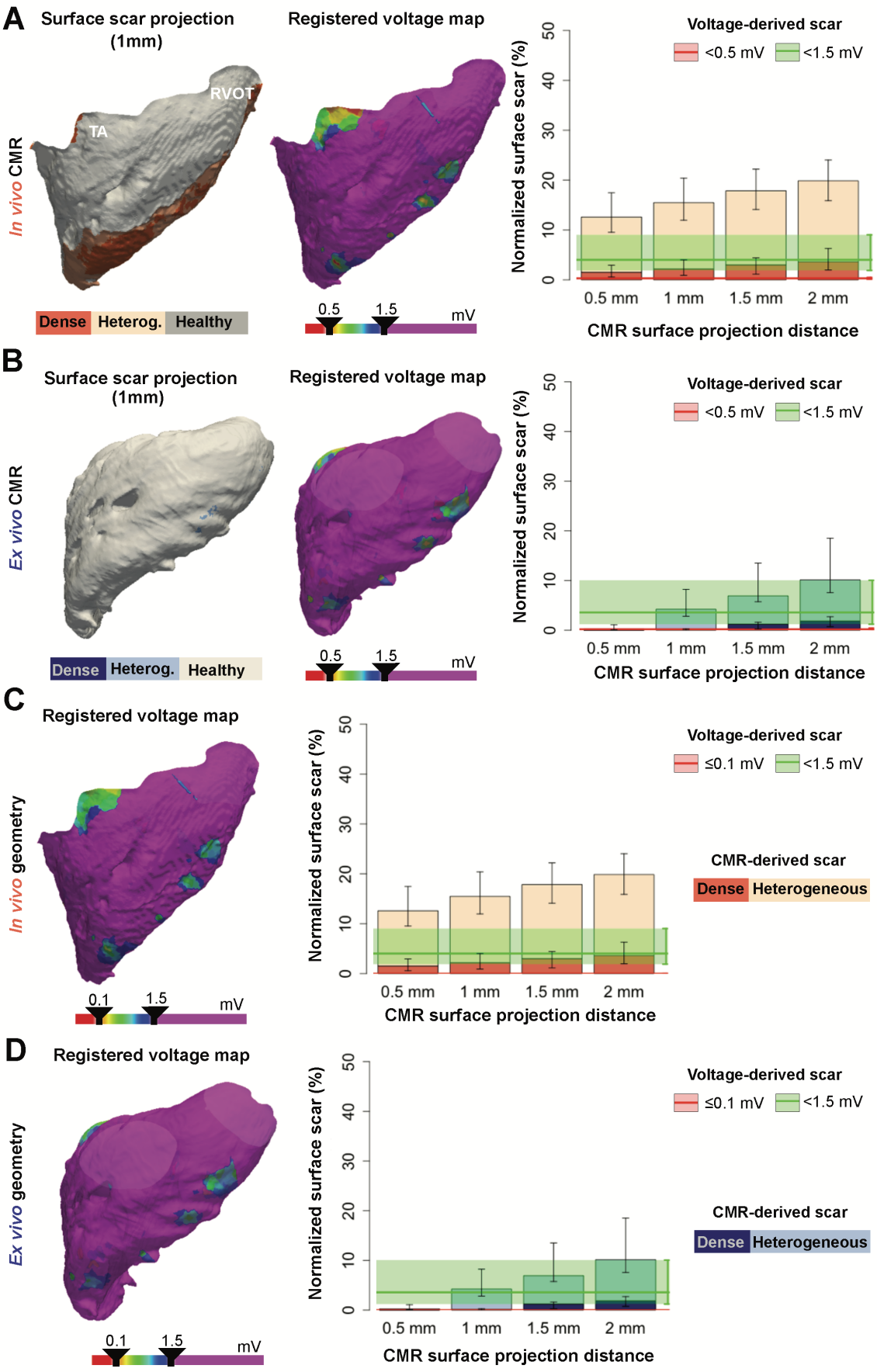
A
Surface scar projection (1mm)
Registered voltage map
In vivo CMR
RVOT
TA
Dense
Heterog.
Healthy
0.5
1.5
mV
Voltage-derived scar
<0.5 mV
<1.5 mV
Normalized surface scar (%)
0.5 mm
1 mm
1.5 mm
2 mm
CMR surface projection distance
B
Surface scar projection (1mm)
Registered voltage map
Ex vivo CMR
Dense
Heterog.
Healthy
0.5
1.5
mV
Voltage-derived scar
<0.5 mV
<1.5 mV
Normalized surface scar (%)
0.5 mm
1 mm
1.5 mm
2 mm
CMR surface projection distance
C
Registered voltage map
In vivo geometry
0.1
1.5
mV
Voltage-derived scar
≤0.1 mV
<1.5 mV
CMR-derived scar
Dense
Heterogeneous
Normalized surface scar (%)
0.5 mm
1 mm
1.5 mm
2 mm
CMR surface projection distance
D
Registered voltage map
Ex vivo geometry
0.1
1.5
mV
Voltage-derived scar
≤0.1 mV
<1.5 mV
CMR-derived scar
Dense
Heterogeneous
Normalized surface scar (%)
0.5 mm
1 mm
1.5 mm
2 mm
CMR surface projection distance

**Figure 6**

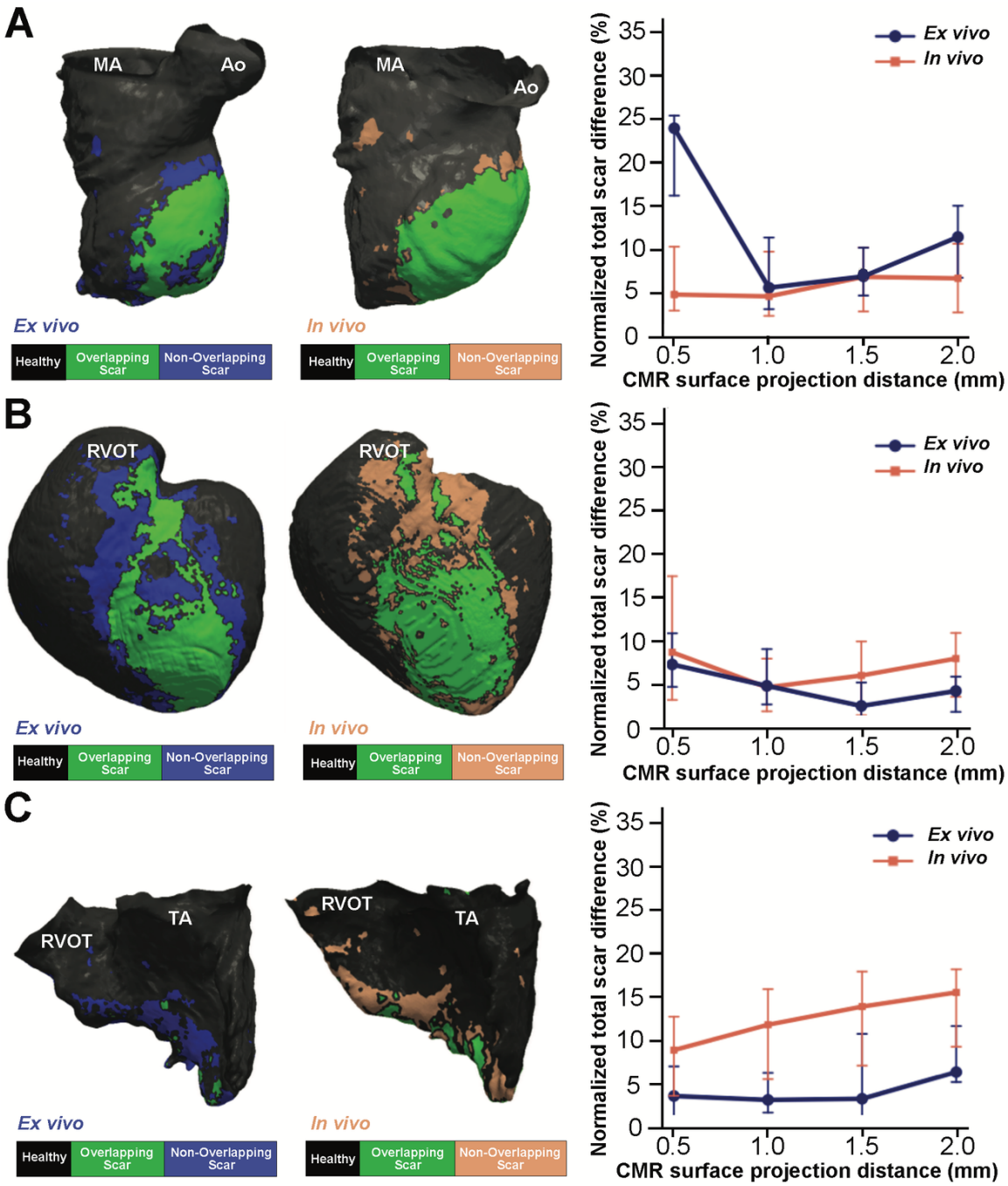
A
MA
Ao
MA
Ao
Ex vivo
In vivo
Healthy
Overlapping Scar
Non-Overlapping Scar
Healthy
Overlapping Scar
Non-Overlapping Scar
Ex vivo
In vivo
Normalized total scar difference (%)
CMR surface projection distance (mm)
B
RVOT
RVOT
Ex vivo
In vivo
Healthy
Overlapping Scar
Non-Overlapping Scar
Healthy
Overlapping Scar
Non-Overlapping Scar
Ex vivo
In vivo
Normalized total scar difference (%)
CMR surface projection distance (mm)
C
RVOT
TA
RVOT
TA
Ex vivo
In vivo
Healthy
Overlapping Scar
Non-Overlapping Scar
Healthy
Overlapping Scar
Non-Overlapping Scar
Ex vivo
In vivo
Normalized total scar difference (%)
CMR surface projection distance (mm)

# Supplementary Data

## Implications of Bipolar Voltage Mapping and Magnetic Resonance Imaging Resolution in Biventricular Scar Characterization after Myocardial Infarction.

Mariña López-Yunta, MSc[a†], Daniel G. León, MSc[b†], José Manuel Alfonso-Almazán, MSc[b], Manuel Marina-Breysse, MD,[b,c] Jorge G. Quintanilla, MSEng, PhD[b,d,e], Javier Sánchez-González, PhD[f], Carlos Galán-Arriola, DVM[b,e], Victoria Cañadas-Godoy, MD, PhD[d,e], Daniel Enríquez-Vázquez, MD[b,d], Carlos Torres, MD[b,d], Borja Ibáñez, MD, PhD[b,e,g], Julián Pérez-Villacastín, MD, PhD[d,e,h], Nicasio Pérez-Castellano, MD, PhD[d,e], José Jalife, MD[b,e,i], Mariano Vázquez, PhD[a], Jazmín Aguado-Sierra, PhD[a*], David Filgueiras-Rama, MD, PhD[b,d,e*]

†Both authors contributed equally to this work.
* Joint corresponding authors.

[a]Barcelona Supercomputing Center (BSC), Barcelona, Spain.

[b]Centro Nacional de Investigaciones Cardiovasculares Carlos III (CNIC), Myocardial Pathophysiology Area, Madrid, Spain.

[c]Agencia Española de Protección de la Salud en el Deporte (AEPSAD), Madrid. Spain.

[d]Instituto de Investigación Sanitaria del Hospital Clínico San Carlos (IdISSC), Cardiovascular Institute, Madrid, Spain.

[e]CIBER de Enfermedades Cardiovasculares, Madrid, Spain.

[f]Philips Healthcare Iberia, Madrid, Spain.

[g]IIS-University Hospital Fundación Jiménez Díaz, Madrid, Spain.

[h]Fundación Interhospitalaria para la Investigación Cardiovascular (FIC), Madrid, Spain

[i]Center for Arrhythmia Research, Cardiovascular Research Center, Department of Internal Medicine, University of Michigan, Ann Arbor, USA

# Supplementary Methods

## Anaesthesia protocol

Anaesthesia induction was achieved by intramuscular ketamine injection (15 mg/kg), xylazine (2 mg/kg) and midazolam (0.5 mg/kg). Then, the pigs were intubated and mechanically ventilated with oxygen (fraction of inspired $O_2$ of 21 %) and anaesthesia was maintained with continuous intravenous infusion of ketamine (2 mg/kg/h), xylazine (0.2 mg/kg/h) and midazolam (0.2 mg/kg/h). A continuous infusion of intravenous amiodarone (150 mg/h) was administered during the infarction procedure to decrease the incidence of malignant arrhythmias.

## Infarct model of myocardial infarction

The studies were conducted in accordance with institutional guidelines and National (ECC/566/2015, RD53/2013) and European (2019/63/EU) regulation guidelines for the care and use of laboratory animals (registered protocol ID: PROEX51/13). The pigs underwent percutaneous catheterization of the left anterior descending (LAD) coronary artery to inflate an angioplasty balloon and occlude the artery for 60 minutes. The balloon was inflated either proximal or distal to the first diagonal branch to generate different infarct sizes and variable scar distributions. Unfractionated heparin (300 mg/kg) was also administered at the onset of the instrumentation. If ventricular fibrillation (VF) arose during the protocol, non-synchronized shocks were delivered with a biphasic defibrillator. After 60 minutes of occlusion, the balloon was deflated and a coronary angiogram was recorded to confirm patency of the coronary artery and reperfusion.

## *In-vivo* parameters of cardiac magnetic resonance imaging

Three-dimensional delayed gadolinium-enhanced sequences were acquired using an inversion-recovery spoiled turbo field echo (IR-T1TFE) with isotropic resolution of 1.5x1.5x1.5 $mm^3$ reconstructed to 0.57x0.57x0.75 $mm^3$. Inversion time was adjusted before acquisition using look-locker scout with different inversion times to ensure proper nulling of the signal from healthy myocardium. The rest of the imaging parameters were repetition time (TR) 2.41ms, echo time (TE) 1.12ms and $10^o$ non-selective excitation angle. All volumes were acquired under free breathing conditions and the acquisition time was reduced using parallel imaging in both phase encoding directions (AP and LR). Inversion time was adjusted before acquisition using look-locker scout with different inversion times to ensure proper nulling of the signal from healthy myocardium.

## *Ex-vivo* cardiac magnetic resonance imaging

Right after euthanasia and heart excision, the hearts were prepared and filled with a 2% warm agarose gel solution via an aortic cannula and a second cannula in the pulmonary artery. A transseptal puncture at the level of the interatrial septum enabled homogenous filling of the four cardiac chambers. The rest of the heart orifices were closed using surgical thread as described elsewhere.[1] Then, the heart was introduced in a custom-designed, watertight plastic flask containing 2% agarose gel that perfectly adjusted to an 8-channel phased array knee coil. A 3D T1 mapping sequence was acquired using a Look-Locker inversion recovery-turbo field echo sequence (TR/TE/Flip Angle=5.9 ms/2.8 ms/7º) with acquired isotropic resolution of 0.6 $mm^3$. Thirty-six inversion times were acquired with a 147-ms gap between them. New inversion pulses were applied every 6 seconds to ensure full signal recovery before consecutive pre-pulses.

**Scar segmentation from *ex-vivo* R1 images**

R1 images were calculated from the 36-inversion times of T1 images using a customized software (IDL 8.1, Boulder, CO) as published elsewhere.[2] Initial segmentation of the myocardium was performed semiautomatically using custom-made software in Matlab, complemented with fine manual segmentation (~28-30 h per heart). Scar segmentation was performed using a modified strategy based on the full-width-half-maximum method to normalize signal intensity to maximum myocardial signal intensity.[3] More specifically, maximum signal intensity was calculated after applying a median filter of 26 neighbouring voxels to avoid detecting spurious single high-intensity voxels. Only the pixels within the left ventricular wall and the infarct region were considered to calculate the maximum signal intensity (Figure S1). All cutoff values from 0.40 to 0.70 of the maximum signal intensity were evaluated to detect the most accurate scar delineation. This step was performed in the original post-contrast R1 images, upon applying a median filter of six neighbours. Spurious heterogeneous scar patches in remote areas (out of the infarct region) with wall thickness >50% of the healthy myocardial wall (excluding the papillary muscles) were filtered to remove potential artefacts. The appropriate threshold for heterogeneous and dense scar tissue was established after evaluation of the myocardial mass classified as scar tissue in two regions; one within the infarct area and a second region within the remote myocardium. The latter enabled us to identify an excessive increase in scar tissue out of the infarct region, which would indicate false positive scar. Interestingly, we observed that above a cutoff value of 0.45 of the maximum signal intensity, the percentage of heterogeneous scar tissue within remote myocardial areas was slightly above 1% (median value), and the main changes in the amount of scar tissue would occur within the infarct region afterwards. Such percentages (~1%) of scar tissue within the remote myocardium are consistent with mild fibrotic remodeling in remote areas.[4]

**Surface projection of 3D scar tissue from CMR images**

Surface scar projection was performed using distance-to-scar maps that were computed from the fine segmentation endocardial and epicardial borders. The maps were generated with a mathematical tool based on Eikonal equations to calculate scar distances to a given surface (Figure S2).[5] Two types of surface maps were generated for each myocardial territory (left ventricular endocardium, right ventricular endocardium and epicardium) to differentiate between dense and heterogeneous scar areas. The first distance-to-scar map projected 3D dense scars and the second map projected the entire segmented scar including the heterogeneous scar. The method enabled us to evaluate sequential scar projection distances for each myocardial territory, either from *in-vivo* or *ex-vivo* CMR images, and understand substrate characterization results from CMR data and bipolar voltage maps. The method avoids projecting averaged intensity signals from myocardial layers at different percentages of the myocardial wall thickness.

**Voltage maps registration onto the CMR geometries**

Each myocardial territory was registered onto the corresponding *in-vivo* and *ex-vivo* CMR geometries. The method consisted of an initial registration of anatomical landmarks manually depicted on each voltage and CMR surface (Figure S3). Five well-distributed landmarks were used for the LV (aortic root, lateral, septal and posterior mitral annulus, and LV apex) and the RV endocardial surfaces (right ventricular outflow tract, lateral and septal tricuspid valve annulus, and anterior and posterior regions of the right ventricular apex), and six landmarks were used for the epicardial surface (epicardial LV apex, proximal and distal LAD coronary artery groove, and right, left and posterior atrio-ventricular groove). During sequential

electroanatomical mapping we positioned 3D dots in areas with equal amplitude of atrial and ventricular electrograms, which facilitated landmark selection on annular regions of the electroanatomical maps. Then, an iterative closest point algorithm was applied to the resulting surfaces using a rigid transformation method.[6] Finally, bipolar voltage data were integrated on the corresponding endocardial or epicardial CMR mesh surfaces using the minimum distance criterion.

**Supplementary references.**

[1] Filgueiras-Rama D, Price NF, Martins RP, Yamazaki M, Avula UM, Kaur K, et al. Long-term frequency gradients during persistent atrial fibrillation in sheep are associated with stable sources in the left atrium. *Circ Arrhythm Electrophysiol* 2012; **5**: 1160-7.

[2] Messroghli DR, Radjenovic A, Kozerke S, Higgins DM, Sivananthan MU, Ridgway JP. Modified Look-Locker inversion recovery (MOLLI) for high-resolution T1 mapping of the heart. *Magn Reson Med* 2004; **52**: 141-6.

[3] Amado LC, Gerber BL, Gupta SN, Rettmann DW, Szarf G, Schock R, et al. Accurate and objective infarct sizing by contrast-enhanced magnetic resonance imaging in a canine myocardial infarction model. *J Am Coll Cardiol* 2004; **44**: 2383-9.

[4] van den Borne SW, Isobe S, Verjans JW, Petrov A, Lovhaug D, Li P, et al. Molecular imaging of interstitial alterations in remodeling myocardium after myocardial infarction. *J Am Coll Cardiol* 2008; **52**: 2017-28.

[5] Sethian JA. A fast marching level set method for monotonically advancing fronts. *Proc Natl Acad Sci U S A* 1996; **93**: 1591-5.

[6] Besl PJ, McKay ND. A method for registration of 3-D shapes. *IEEE Transactions on Pattern Analysis and Machine Intelligence* 1992; **14**: 239-56.

## Supplementary Figures

**Figure S1**

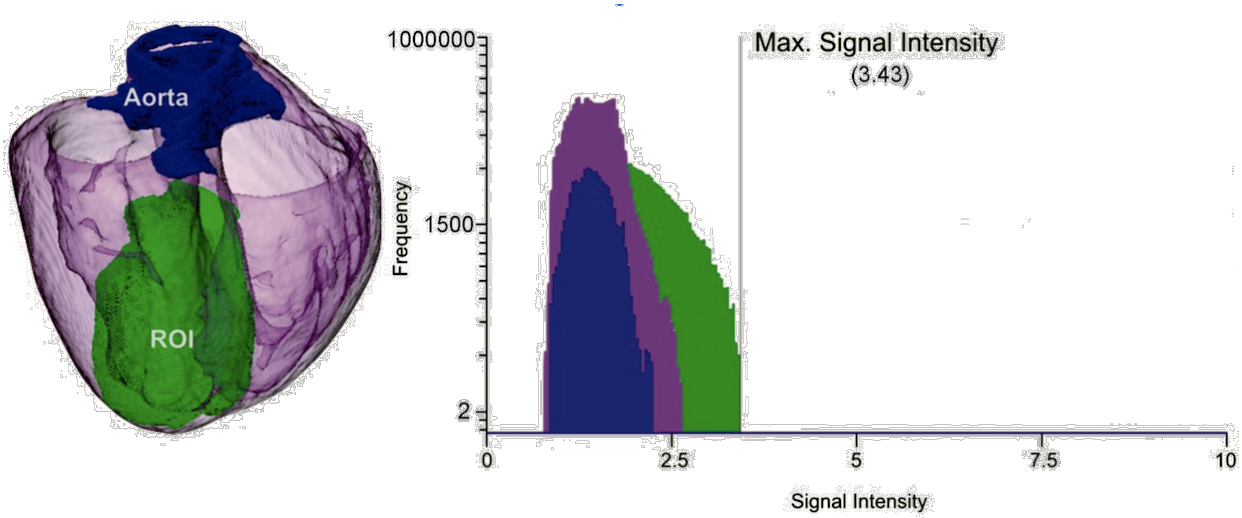


**Figure S1. Calculation of the maximum signal intensity within the infarct region.** The infarct region (in green) of interest (ROI) was manually delineated to calculate the maximum signal intensity value, which was used as reference value to establish the criteria for scar tissue. Blue colour codifies the aorta and fibrotic annuli.

**Figure S2**

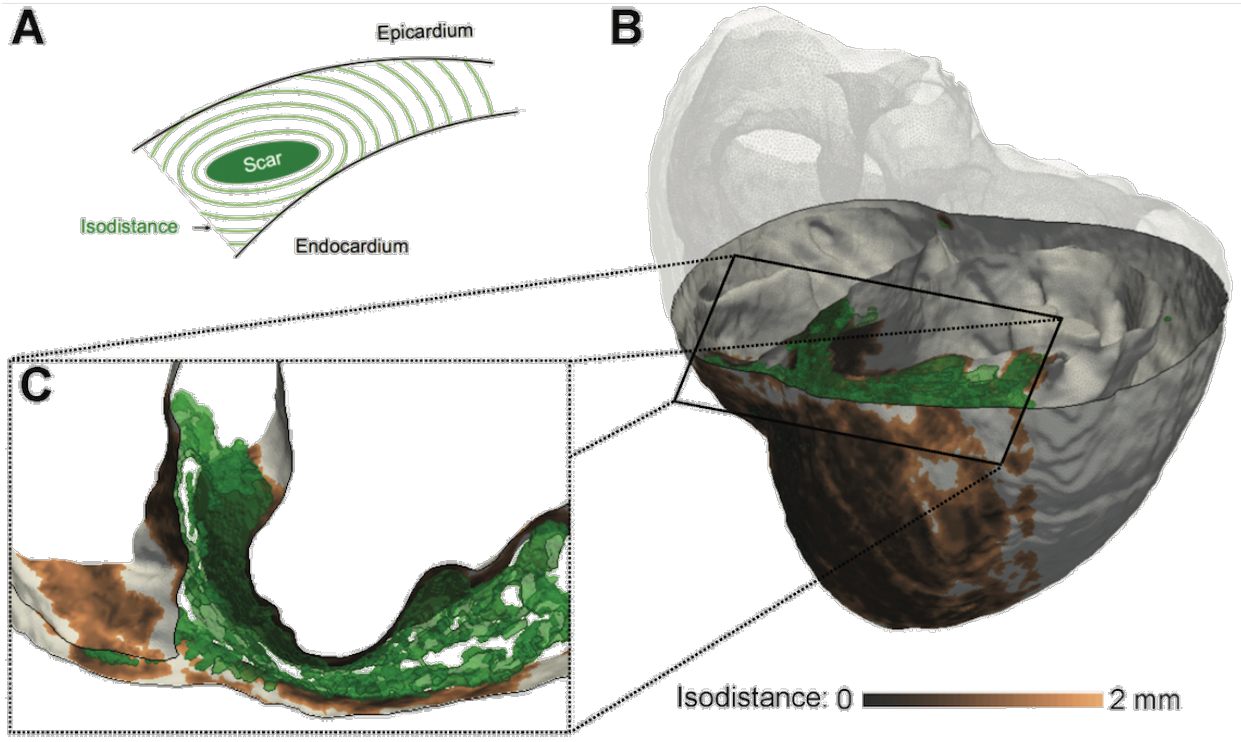


**Figure S2. Surface projection of 3D scar tissue from CMR images. A**, distance-to-scar maps were generated with a mathematical tool based on Eikonal equations to calculate scar distances to a given surface. **B,** sample 3D CMR-based reconstruction showing colour-coded distances to the scar. **C,** Zoom in of the scar region showing color-coded distances to the scar. CMR: cardiac magnetic resonance.

**Figure S3**

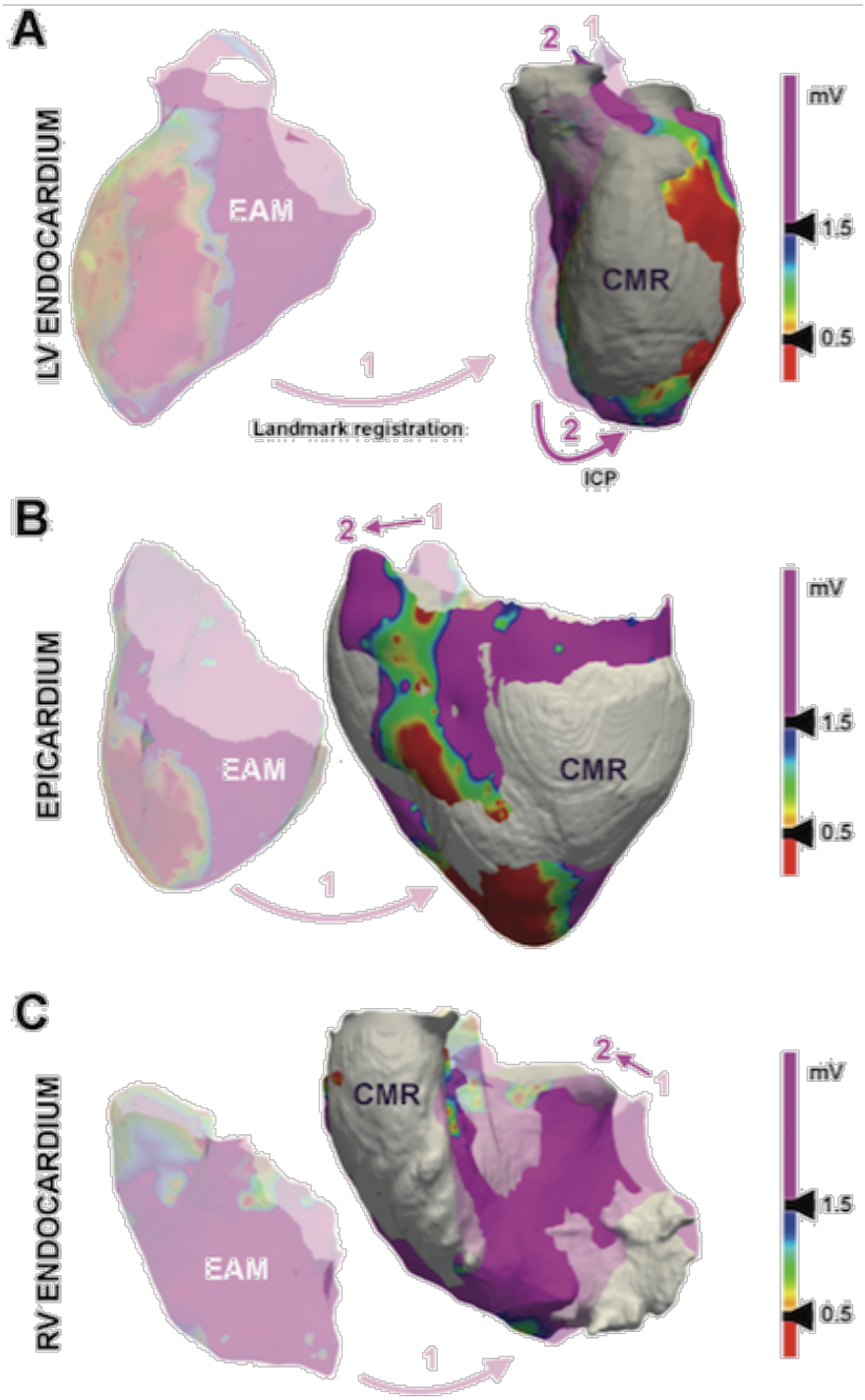


**Figure S3. Registration of voltage-derived maps onto CMR geometries. A, B, C,** registration process of voltage-derived maps of the left ventricular (LV) endocardium (A), epicardium (B) and right ventricular endocardium (C) onto the each specific CMR geometry. Step 1: initial registration of anatomical landmarks. Step 2: iterative closest point (ICP) algorithm. CMR: cardiac magnetic resonance.

**Figure S4**

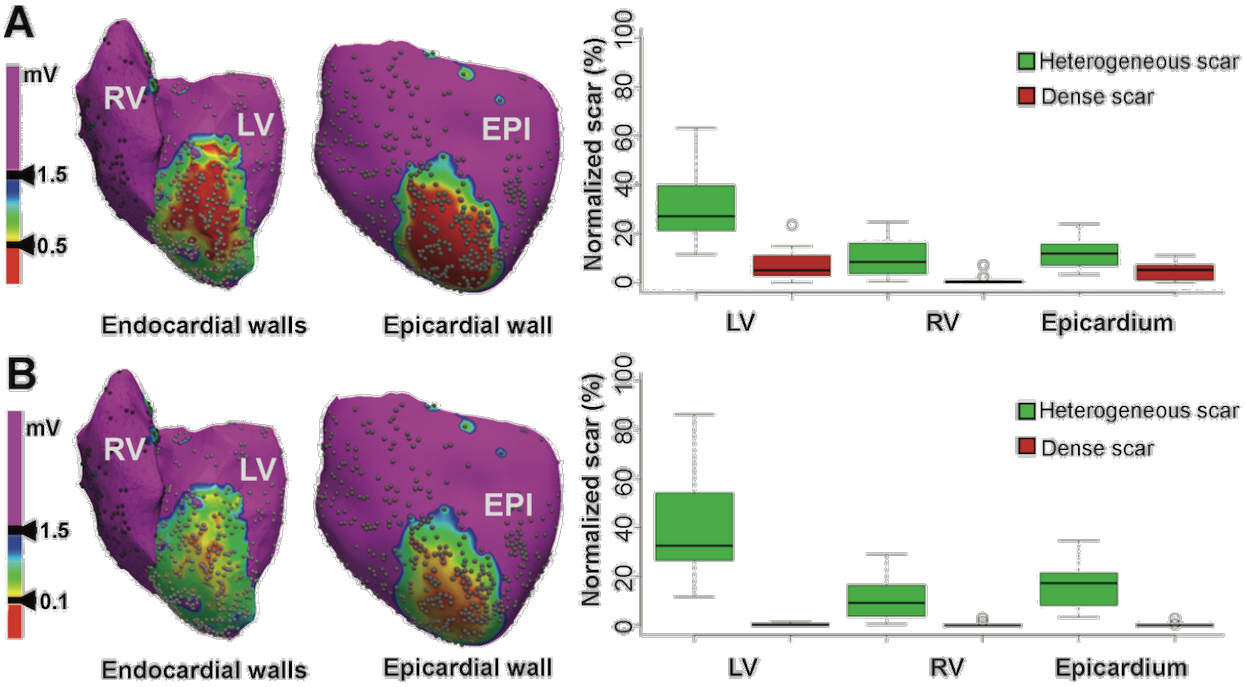


**Figure S4. Effect of the cut-off criterion to assign very low voltage areas. A,** on the left, representative sample case using conventional low (≤1.5 mV) and very low (<0.5 mV) voltage criteria. Grey dots indicate acquisition points. On the right, scar tissue classified as heterogeneous (green) or dense (red) scar in the left ventricle (LV), the right ventricle (RV), and the epicardium (N=10). **B,** on the left, same representative case as in panel A after adjusting the very low voltage cutoff to ≤0.1 mV, which dramatically decreased dense scar tissue in the entire group of pigs (on the right).

**Figure S5**

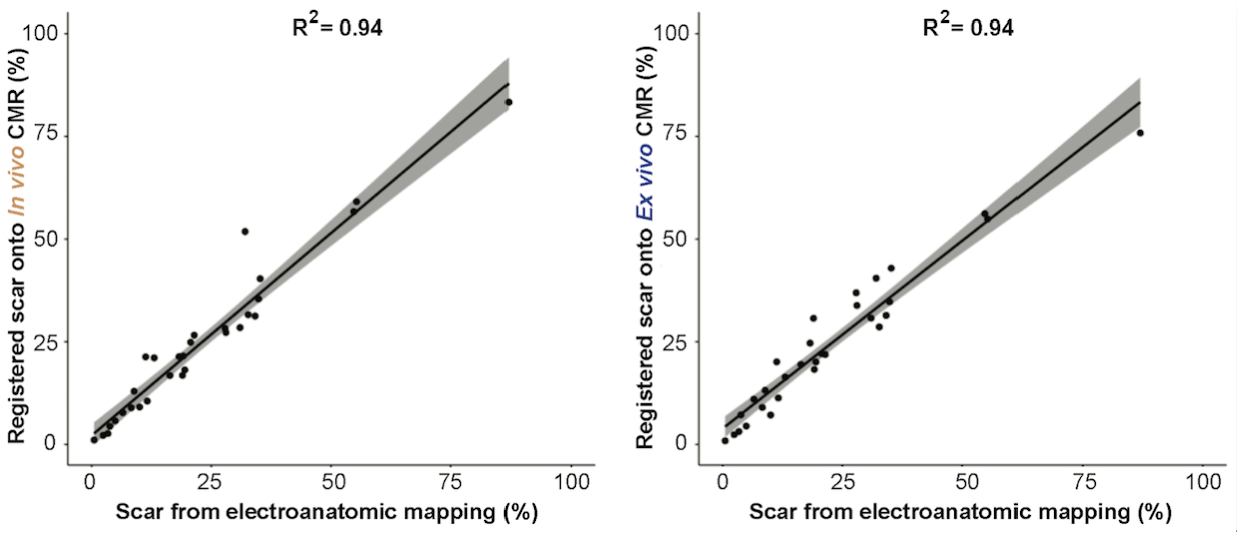


**Figure S5. Correlation analysis of voltage maps registration onto CMR geometries. A,** Pearson correlation coefficient between voltage-derived scar on the electroanatomic meshes and the registered voltage-derived scar onto the *in-vivo* CMR geometries. **B,** Pearson correlation coefficient between voltage-derived scar on the electroanatomic meshes and the registered voltage-derived scar onto the *ex-vivo* CMR geometries. CMR: cardiac magnetic resonance.

**Figure S6**

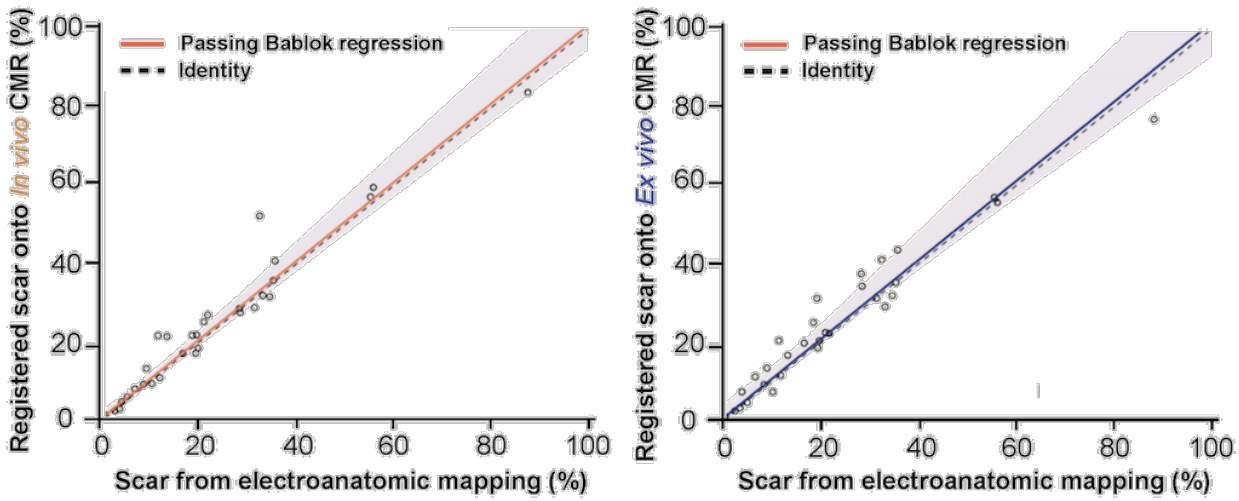


| (n= 30) | Registered scar onto | |
|---|---|---|
| **Passing Bablok regression** | ***In vivo* CMR** | ***Ex vivo* CMR** |
| Intercept | **0.599** (-0.675, 2.069) | **0.537** (-0.701, 3.885) |
| Slope | **1.005** (0.935, 1.136) | **1.010** (0.900, 1.196) |

**Figure S6. Passing Bablock analysis of voltage-derived scars registration onto CMR geometries.** On the top, the regression shows almost identical normalized scar after the registration on both in-vivo and ex-vivo CMR geometries. On the bottom, the data did not show any systematic deviation after the registration process. CMR: cardiac magnetic resonance.

**Figure S7**

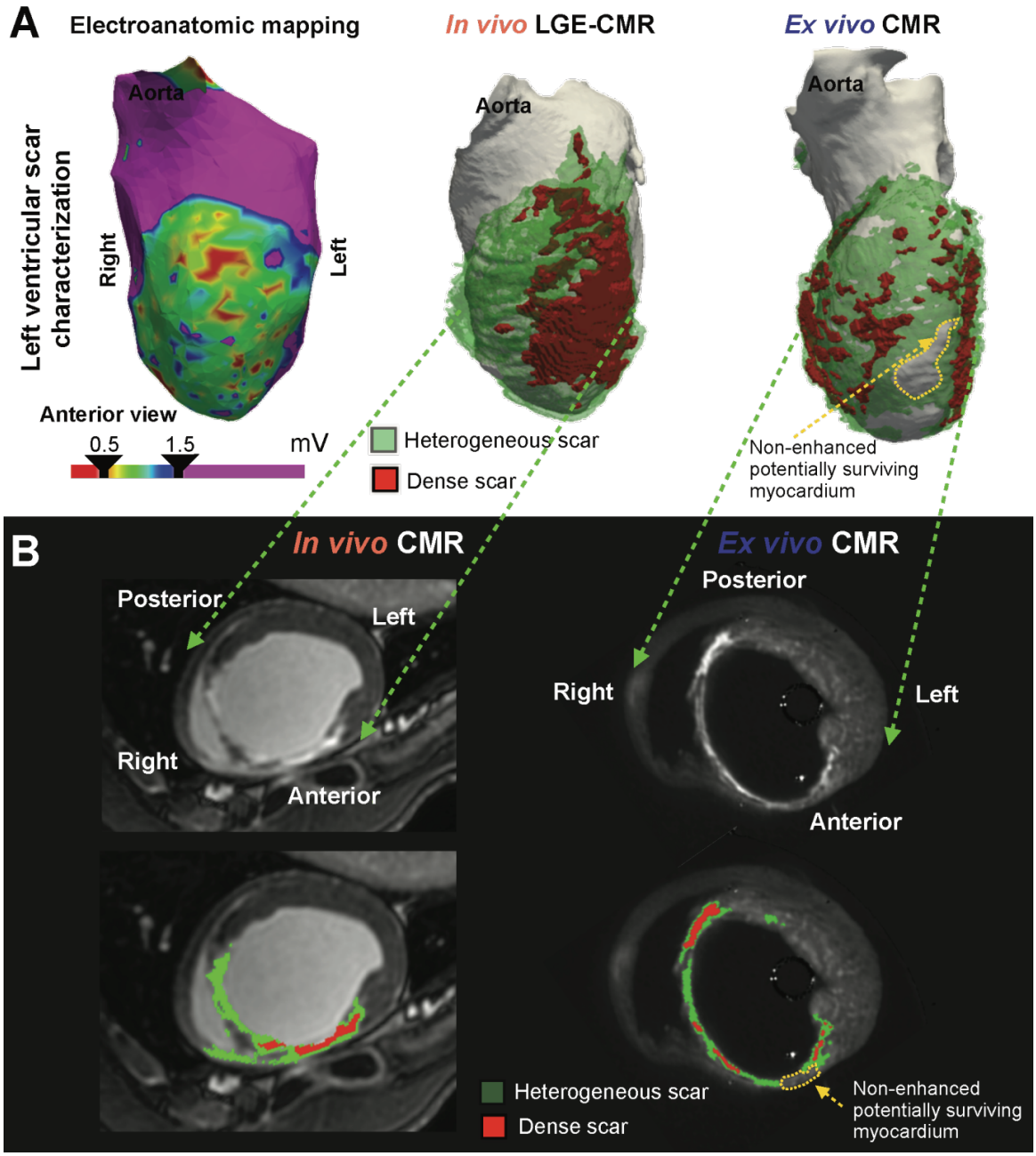


**Figure S7. Representative case of non-enhanced potentially surviving regions within the infarct territory. A,** 3D left ventricular scar characterization using bipolar voltage mapping with a 3.5-mm tip catheter (on the left), *in-vivo* delayed-enhancement cardiac magnetic resonance (LGE-CMR) imaging (middle panel), and *ex-vivo* high-resolution postcontrast T1 mapping (on the right). *Ex-vivo* CMR images identified a non-enhanced region with potentially surviving myocytes (yellow dashed line) within the low voltage territory on the electroanatomical map and the dense scar region in the *in-vivo* LGE-CMR. **B,** Short axis CMR slices showing an *ex-vivo* CMR-based non-enhanced region (yellow dashed line) within a predominantly dense scar territory on the in-vivo LGE-CMR image.

**Figure S8**

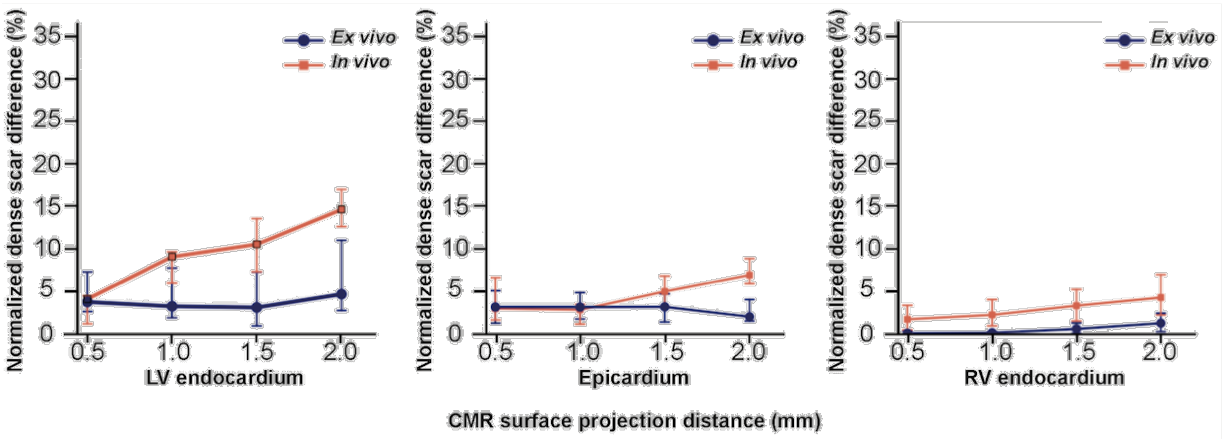


**Figure S8. Dense Scar differences among registered voltage maps and CMR images at different surface projection distances.** Normalized dense scar differences (|voltage-derived dense scar – surface projected CMR dense scar| / LV, RV or epicardial surface) using sequential surface projection distances from *in-vivo* and *ex-vivo* CMR images. CMR: cardiac magnetic resonance. LV: left ventricle. RV: right ventricle.